Closer Look at the fMRI Data Analysis Pipeline and its Application in Anesthesia Resting State Experiment

by

Andrew Hyungsuk Song

B.S., Massachusetts Institute of Technology (2015)

Submitted to the Department of Electrical Engineering and Computer Science
in partial fulfillment of the requirements for the degree of

Master of Engineering in Electrical Engineering and Computer Science

at the

MASSACHUSETTS INSTITUTE OF TECHNOLOGY

June 2016

Author .....
Department of Electrical Engineering and Computer Science
Aug. 29th, 2016

Certified by .....
Emery N. Brown
Edward Hood Taplin Professor of Medical Engineering and of Computational Neuroscience
Thesis Supervisor

Accepted by .....
Chris J. Terman
Chairman, Department Committee on Graduate Theses

Closer Look at the fMRI Data Analysis Pipeline and its Application in Anesthesia Resting State Experiment

by

Andrew Hyungsuk Song

Submitted to the Department of Electrical Engineering and Computer Science
on Aug. 29th, 2016, in partial fulfillment of the
requirements for the degree of
Master of Engineering in Electrical Engineering and Computer Science

Abstract

The main focus of the thesis is the resting state fMRI data analysis, with much emphasis on the anesthesia fMRI experiments. Under this central topic, three separate themes are developed: resting state fMRI data analysis overview, improved denoising techniques, and application to the Dexmedetomidine experiment data. In the first part, important and confusing resting state data analysis steps are explored in-depth, focusing on how and why the pipeline is different from that of the task-based fMRI. In the second part, the Principal Component Analysis (PCA) based denoising technique is introduced and compared against the conventional fMRI denoising techniques. Finally, with the PCA denoising technique, the functional connectivity of the brainstem with the brain is assessed for the Dexmedetomidine-induced unconscious subjects. We found that the functional connectivity between the Locus Ceruleus (LC) in the brainstem and the Thalamus & Posterior Cingulate Cortex (PCC) is the neural correlates of the Dexmedetomidine-induced unconsciousness.

Thesis Supervisor: Emery N. Brown
Title: Edward Hood Taplin Professor of Medical Engineering and of Computational Neuroscience

Acknowledgments

First of all, I would like to thank Professor Emery Brown for giving me an opportunity to work on the amazing topic of unconscious brains and providing me with profound insights on the topic from both the neuroscience perpsective and the statistical perspective. Professor Brown has given me the freedom to seek out challenging problems that align with my electrical engineering background and helped me navigate through difficult obstacles. I am very much looking forward to working with him in upcoming years during my Ph.D. Next, I would like to thank Dr. Oluwaseun Akeju for his unconditional mentorship over the past year. As a researcher/doctor, he always brought his clinical insights on the table and encouraged me to look at the problems from various perspectives. As my supervisor, he tried hard to make sure that I get as much and diverse experience as possible, from collaborating with other research groups to peer reviewing the works of the others. Next, I would like to thank Dr. Marco Loggia, for teaching me everything about the fMRI (and Neuroimaging in general) Data analysis, when I came as a new student. Without his help and resources, it would not have been possible for me to explore other aspects of the data analysis, which are among the central themes of this thesis. I also want to thank all the members of the Neuroscience Statistics Research Laboratory at MIT, for their support throughout the M.eng progam. Lastly, I want to thank my parents and my brother for their unconditional support and love.

Contents

List of Figures

Chapter 1

Introduction

The question of what it means to be conscious and unconscious has been around for very long, initially more as a philosophical conundrum. Questions, such as what causes one to become unconscious, whether it is sleep or serious medical conditions such as coma or vegetative state, and what happens during such unconsciousness, has remained mysterious. It is without a doubt that these questions were of great interests to the scientists. Despite all the curiosity and the endeavors, the research progress has been stagnant for the previous few centuries mainly for two reasons. First, there were no safe and easy mechanisms through which the subject's level of consciousness could be controlled. Second, there were no sophisticated tools to probe the functional brain states non-invasively. Although invasive probing prodcedures have been performed on animals, such as monkeys and rats, there were no direct evidences linking these findings to the humans.

With the advent of anesthesia practice in the late 19th century, the first problem was partially solved. With different drugs, it was possible to put humans and animals in different conscious states in a reversible manner, such that the subjects could be woken up from the unconsciousness [1]. Moreover, with the recent development of the anatomical and functional neuroimaging techniques, scientists have finally been able to examine the functional brains states non-invasively. For example, Electroencephalogram (EEG) enabled tracking the brain signals in high temporal resolution

(milliseconds scale), which helped scientists to discover several brain signatures that indicated transition from one brain state to the other. Functional Magnetic Resonance Imaging (fMRI) on the other hand, helped locate which brain regions are functionally activated or deactiviated throughout the different levels of consciousness, with high spatial resolution of millimeter scale. With the means of controlling and monitoring the brain states, scientists have been able to make significant advances in uncovering the mysteries of the consciousness.

This thesis also started out as an effort to examine how the brain states change in different levels of consciousness, specifically under a specific drug called dexmedetomidine. There were several reasons behind the choice of Dexmedetomidine as the drug of interest. First, Dexmedetomidine is an appealing choice for investigating the neural circuits behind alternating consciousness, as the drug selectively targets the presynaptic α2-adrenergic receptors on neurons projecting from the locus ceruleus to the pre-optic area [2]. This selectivity allows researchers to easily trace the mechanisms behind the Loss of Consciousness (LOC) and the Recovery of Consciousness (ROC) due to Dexmedetomidine, as shown in Figure 1-1. Second, it has been shown that the neurophysiological signatures of the unconscious state produced by Dexmedetomidine closely resemble those of the non-Rapid Eye Movement II sleep. Therefore, Dexmedetomidine has a huge clinical potential for the sleep research and therapies. For this thesis, we focus specifically on the Lous Ceruleus, as this is the main site where the transition to the unconsciousness begins.

Along the course of the project, I made two observations that intrigued my engineering curiosity, and have since diversified the aims of the thesis. First observation was that many of the neuroimaging researchers, driven by the clinical aspects of their studies, did not put as much emphasis on the data analysis as experiment design and data collection, settling on the popular methods used by the community without considering how the predefined analysis pipelines can affect their results. In other words, most of the interest was on **how** the data could be analyzed, not **why** the

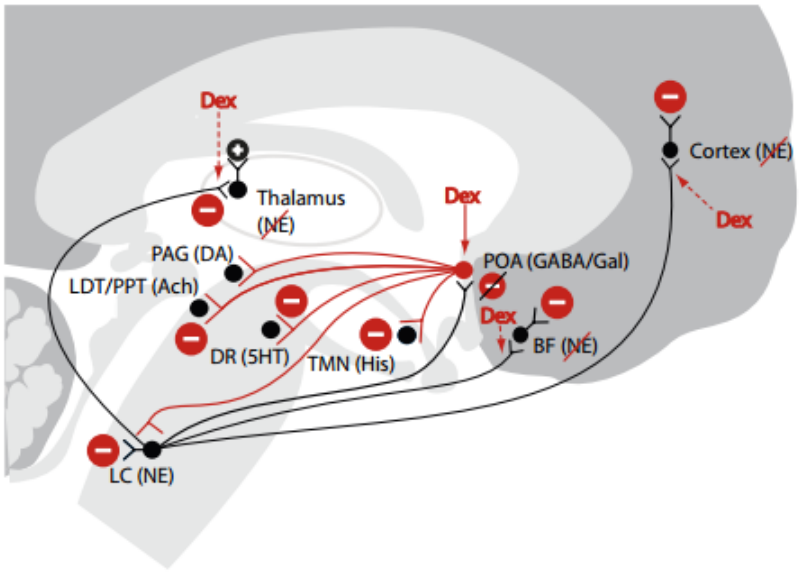

Figure 1-1: The neural mechanism behind Dexmedetomidine. Reproduced from [2]

data could be analyzed in such a way. Moreover, the resources on fMRI data anlysis, such as forums and tutorials, were scarce for the resting-state fMRI paradigm, as the majority was focused on the task-based paradigm.

Another observation was that the current denoising techniques still had lots of room for improvements, even after the general denoising problem being of interest for several decades. What excited me about the denoising problem, in the fMRI context particularly, was that the solutions not only required statistical and signal processing expertise, but also benefited a lot from the knowledge of the underlying neuroanatomy and the brain dynamics. I learned that, with the advance of the neuroimaging tools and the expansion of our knowledge of the brain, the denoising techniques for neuroimaging would only get better. Throughout the thesis, I tried to establish the links between the engineering (denoising) and the science (neuroscience).

This brings us to the three main objectives that the thesis tries to achieve. First is to provide a general overview of the entire data analysis pipeline for fMRI experiments, with emphasis on the resting-state experiments (rs-fMRI) and develop some

insights in understanding the fundamental principles of the data analysis of not only the fMRI, but also the neuroimaging field in general. Section 2.1 $\sim$ section 2.4 contains this first part. Although these sections cover basic concepts in the fMRI data analysis, it is assumed that the reader is already familiar with these concepts and also with the task-based fMRI. The second objective is to propose and evaluate improvements on the existing data analysis pipelines. The discussion is centered around the principal component based approach and how its performance compares against the conventional preprocessing pipelines. Moreover, this discussion includes how the understanding of the brain can help improve the methods. Section 3.1 $\sim$ section 3.2 contains this second part. Finally, the last aim is to analyze the fMRI data of subjects under dexmedetomidine using the proposed pipeline. This analysis is based on the fMRI dataset collected from the 15 subjects in the previous Dexmedetomidine study [2]. As such, the detailed imaging protocols are not mentioned in this thesis. Section 4.1 contains this final part.

Chapter 2

fMRI Data Analysis

2.1 Resting state fMRI Overview

2.1.1 Task-based & Resting State fMRI paradigm

The task-based fMRI aims to test whether certain brain region is activated/deactivated by a given task. Since a task paradigm is defined explicitly, it is easy to obtain the reference signal for the experiment, by convolving the experiment (stimulus) time-frame with the canonical Hemodynamic Response Function. The reference signal is essentially noise-free.

On the other hand, the aim of the resting state fMRI is to observe what regions are instrinsically connected. For this experiment, there are no external stimulus and the subjects are instructed to remain still for the whole scan, to minimize the confounding factors for assessing the intrinsic functional connectivity. Nevertheless, the resting state is loosely defined, as it is unclear what the subjects might be thinking as they remain still and how these will affect the results. Since the aim is to assess the connectivity between the brain regions, the reference signal is the averaged BOLD signal of the region of interest (ROI). Since the reference signal contains noise, denoising the brain signal is important, perhaps even more so than the task-based paradigm. Past resting state fMRI studies revealed the existence of several intrinsic

functional networks, such as Default Mode Network (DMN) [3].

2.1.2 Combining Anesthesia & fMRI

Combined with the anesthesia practice, fMRI experiments can reveal how several functional networks, such as thalamo-cortical connection and cortico-cortical connection, change when subjects are in different levels of consciousness. Since there are no external stimulus (other than the verbal stimuli to check whether the subject is unresponsive) and the subjects are not required to complete any task throughout the experiment, this is regarded as a branch of resting-state fMRI. Typically three sets of scans are taken for anesthesia resting state fMRI.

1) **Pre** - Before Anesthesia Injection: This scan is a conventional resting state fMRI experiment and serves as a baseline scan for the experiment.
2) **Peri** - After Loss of Consciousness (LOC): This scan is taken after the subject has lost consciousness and does not respond to external stimuli.
3) **Post** - After Recovery of Consciousness (ROC): This scan is taken after anesthesia injection has stopped and the subject recovers consciousness. This is likely to produce different results from the baseline scan, as different parts of the brain might take longer to recover fully.

The second and the third set of scans are also considered resting state scans, as the subjects are still and do not perform any tasks. For the Dexmedetomidine study, 6:15 min BOLD fMRI scans were performed for all three conditions.

One limitation of the anesthesia fMRI studies is that the imaging modality is not able to track the change of brain states dynamically, unlike EEG. Part of the reason is that LOC and ROC typically happens within matter of miliseconds, while the typical repetition time (TR) for fMRI is on the order of seconds. Moreover, the scans collected in each state are summarized to a set of parameters for further statistical analysis, obliterating the temporal information within each brain state. Recently,

there have been attempts to track dynamical brain state change using wavelet transforms, but it is still unclear whether the results yield meaningful interpretations [4].

2.1.3 Functional Connectivity

The functional connectivity is defined as the statistical dependencies among spatially remote neurophysiologic events, which was first explored in the context of multiunit electrode recordings [5]. This is to be differentiated from the *effective connectivity*, which measures the influence one neuronal system exerts the other. To state it differently, functional connectivity is concerned with the relation, whereas the effective connectivity is concerned with the causation [6]. The functional connectivity metric is important in the resting state fMRI context, as the main objective of the experiments is to observe the change of functional networks, or functional connected regions, of the brain. The fairly loose definition of the statistical dependency welcomes several different interpretations of the functional connectivity, such as temporal correlation, coherence, mutual information, and etc. Here, we only look at the most popular measure, the temporal correlation.

Temporal Correlation

Temporal correlation of BOLD timeseries between two different regions is the most widely used metric for the functional connectivity. Among several temporal correlation metrics, the Pearson product-moment correlation coefficient is the most popular choice. For a given pair of N length voxel timeseries, $\mathbf{x_i} = [x_{i,1}, x_{i,2}, \cdots, x_{i,N}]$ and $\mathbf{x_k} = [x_{k,1}, x_{k,2}, \cdots, x_{k,N}]$ where i and k are two different voxels, the pearson correlation, r, is given as

$$r = \frac{\sum_{t=1}^{N}(x_{i,t} - \overline{x_i})(x_{k,t} - \overline{x_k})}{\sqrt{\sum_{t=1}^{N}(x_{i,t} - \overline{x_i})^2}\sqrt{\sum_{t=1}^{N}(x_{k,t} - \overline{x_k})^2}} \tag{2.1}$$

, where $\overline{x}$ is the average timeseries. High correlation (high $\mid r \mid$, closer to 1) would indicate that the two regions have strong functional connectivity, whereas low corre-

lation (low $\mid r \mid$, closer to 0) would indicate the opposite. It is important to note that r could be negative, indicating anti-correlation between two regions. High degree of anti-correlation would indicate that the two regions are functionally related, in an opposite manner. The entire field of anti-correlation between two different networks, such as that of task-positive and task-negative networks, stem from the fact that the correlation is negative [3]. Typically, an averaged BOLD signal from a Region of Interest (ROI) is extracted and is correlated with every other voxel within the brain to analyze which regions are functionally connected with the ROI.

Since the ROI BOLD signal is used as the reference signal for the whole-brain correlation analysis, it is important that the reference signal has as much noise removed as possible. Partially denoised reference signal would lead to spurious correlation measures. Several physiological noises, such as respiratory or cardiac movement, affect and modulate the BOLD signal globally within the brain - Thus failure to acknowledge such sources leads undesirable results. For the task-based fMRI framework, denoising brain BOLD timeseries, although still important, does not have as huge improvement in terms of accuracy, since the reference signal in this case is essentially noise-free.

One of the main limitations of the temporal correlation is that the Hemodynamic Response Function is not likely to be the same in different brain regions. Even if the underlying neural activities are the same, the different HRF would result in different BOLD signal, which would produce incorrect functional connectivity results. Nevertheless, this is not so much of an issue in the resting state context, since it is impossible to ascertain what the underlying neural activities are in the resting state. Therefore, the focus is less on the underlying neural signals, but more on the measured BOLD signal and how these signals are temporally correlated to each other.

2.1.4 Hypothesis Test

As with the majority of scientific experiments, the main objective of the neuroimaging experiments is to test a hypothesis. In fMRI experiments, there are largely two catergories of hypothesis. In task-related fMRI experiments, the aim is to find the brain regions that are activated/deactivated when a subject peforms certain tasks. In other words, the experiment tests the hypothesis that a specific voxel (or region) gets activated/deactivated when the subject performs the tasks. These tests are performed in every voxel (or region) of the brain, and only the statistically significant parts are regarded as relevant to the task, albeit with some probability of error. This is same in the resting state context. The hypothesis for the resting state would be whether the ROI is functionally connected to a specific voxel (or region) or not. If the test is statistically significant, it would mean that the ROI is functionally connected to the voxel (or region) to some degree.

Of course, the hypotheses can be more complicated when several signals are involved. For example, a hypothesis could be that the first signal of interest (i.e. stimulus signal) has more effect than the second signal of interest (i.e. feedback signal) in certain region. This would require a significant test for the *contrast* of the effect sizes, namely $\hat{\beta}_1 - \hat{\beta}_2$, where $\hat{\beta}_1$ and $\hat{\beta}_2$ are the parameter estimates for the first and the second signal of interest, respectively. The null hypothesis, H_0, would be $H_0 : \beta_1 - \beta_2 = 0$ and the alternative hypothesis, H_1, would be $H_1 : \beta_1 - \beta_2 \neq 0$. In general terms, $\mathbf{c}\hat{\beta}$ is used to denote the contrast of parameter estimates (COPEs), where $\mathbf{c}$ is the $1 \times p$ contrast vector and $\hat{\beta}$ is the $p \times 1$ parameter estimates vector. For the example, $\mathbf{c} = [1 \ -1 \ \cdots, 0]$ and $\hat{\beta} = [\hat{\beta}_1, \hat{\beta}_2, \cdots, \hat{\beta}_p]^T$.

For most of the neuroimaging studies, the null hypothesis tests whether a given test statistic at any specific level, be it a single subject or a whole group, equals 0. It is definitely possible to have the null hypothesis test the statistic against any non-zero constant d. However, this is not used as much in the practice. First, the null dis-

tribution is different. For example, in case of the T-test, the null distribution would be noncentral T-distribution with a specific non-centrality parameter. Second, since the effect size of the experiment is often unknown, it is not trivial what d means. In other words, it is hard to interpret what the absolute value of $\mathbf{c}\hat{\beta}$ means. In contrast, regardless of the units or scale factors, the formulation $\mathbf{c}\hat{\beta} = 0$ is an easily interpretable hypothesis. Therefore, unless the researcher has absolute confidence in what the effect size and the null hypothesis are, it is advised to design the null hypothesis to be a comparsion of the test statistic against 0.

To conduct hypothesis testing, one needs to define a test statistic and a sampling distribution that can be used as a null distribution and from which the threshold for statistical significance can be calculated. There are two different approaches for constructing the sampling distribution for the hypothesis testing, parametric and non-parametric approach. The standard procedure for the hypothesis testing is as follows:

1. Using the General Linear Models (GLM), run regression and obtain the test-statistic.
2. With the sampling distribution as the null distribution for the hypothesis, calculate the p-value for the test-statistic.
3. If the p-value of the test statistic is lower than the p-value threshold, the result is statistically signficant and the null hypothesis is rejected. If the p-value is higher than the threshold, it is not statistically significant.
4. Repeat Step 1-3 for the entire brain voxels (or regions).

There are two important consequences of this general procedure. The first is the multiple comparisons problem. Since this procedure is repeated many times (typically as many as the number of voxels), the test statistics of some voxels are expected to have p-values less than the threshold, making them statistically significant, even though they are sampled from the null distribution. The second consequence is that the p-value threshold for the statistical significance needs to be carefully chosen, since

the significance of the region is sensitive to the threshold. This sensitivity gives rise to an important question in hypothesis testing - Which level of statistical signficance should be used for the experiment, to produce the *best* results?

In Hypothesis Testing context, it turns out that there is no such golden threshold - there is always a tradeoff between the number of false positives and the number of false negatives. If the threshold is higher, it is less likely that the null regions (or voxels) become false positives (Type I Error). At the same time, it is more likely that the regions where the actual effects exist become false negatives. The logic is similar for the lower threshold, where the false negative regions are less likely but false positives are more likely. Figure 2-1 is an example of how different thresholds lead to different interpretations. This is the Locus Ceruleus seed functional connectivity contrast image between peri-Dex and pre-Dex for threshold of $z = 1.5$ and $z = 3.1$, for the left and the right image, respectively. With lower threshold, $z = 1.5$, there is loss of specificity, due to the increased number of false positive voxels. Surely, we can conclude that all the blue regions, Posterior Cingulate Cortex, Precuneus Cortex, and Medial Parietal Frotal Cortex, have decreased functional connectivity with the LC seed. However, this is a very loose interpretation, due to the lack of specificity. Nevertheless, one can argue that it is a safe conclusion, since despite the false positives, it is unlikely that there exists regions other than the indicated ones that have decreased functional connectivity. With higher threshold, $z = 3.1$, the result is very specific to the posterior cingulate cortex. Nevertheless, this tight threshold could leave out some regions that are important. The standard significance p-value threshold in the neuroimaging literature is either $p = 0.05$ or $p = 0.001$, which corresponds to the z-stat threshold of $z = 2.3$ and $z = 3.1$, respectively, in normal distribution. It is important to note that in fMRI data analysis, because of the multiple comparisons problem, $z = 2.3$ and 3.1 are not the final thresholds. In voxel-based correction scheme, this z-stat significance threshold is increased, whereas in the cluster-based correction scheme, there is an additional significance threshold for clusters. The details will be covered in section 2.3.

In essence, most of the efforts to increase the SNR of fMRI data and produce

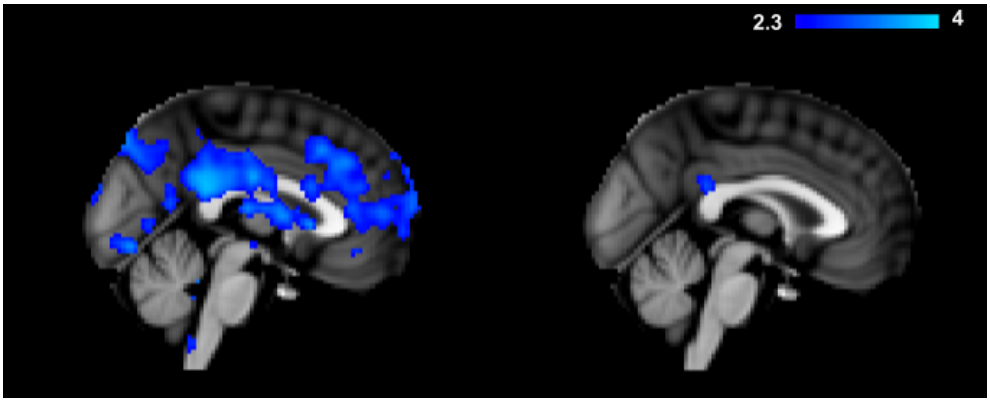

Figure 2-1: Functional Connectivity contrast image between peri-Dex and pre-Dex with Locus Cerulues seed for different thresholds. The left image is thresholded at $z = 1.5$ and the right image is threshold at $z = 3.1$

more accurate results can be traced to trying to solve various problems arising from the hypothesis testing framework. The issues of temporal autocorrelation are important since the test statistic can no longer be assumed to follow the easily computable and familiar T, χ^2, or z distribution under null hypothesis. Several variants of the parametric or non-parametric approaches aim to address the null distribution problem. The multiple comparisons problem arises due to the sheer number of hypothesis tests. Finally, denoising methods of the fMRI signal aim to produce more accurate test-statistics, to reduce the number of false positive and false negative regions.

2.1.5 Interpreting the z-stat and functional connectivity

In the resting state paradigm, the z-stat of a voxel/cluster would indicate the statistical significance of the functional connectivity between that voxel/cluster and the ROI. This is where the misinterpretation often occurs. If a voxel/cluster passes the statistical significance threshold, it means that the null hypothesis that the ROI and the voxel/cluster is not functionally connected can be rejected with high probability. But this does not clearly tell us to what degree these two are functionally connected, other than that it is non-zero. Recall that the z-stat (or t-stat for that matter) is

formed as $\frac{COPE}{variance\ of\ COPE}$. This implies that a high z-stat can be caused by 1) high COPE, 2) small variance of COPE, or 3) combination of both. This is where the confusion often arises. Based on the magnitude of the z-stats for each voxel/cluster, it is tempting to draw conclusions about the strength of the functional connectivity with the ROI and the rest of the brain, based on the magnitude of the z-stats for each voxel/cluster. However, one must acknowledge that the variance can be a major factor influencing the z-stat as well. It could be that a certain region/voxel has high z-stat as the variance of COPE is really small, when in fact the COPE, the strength of the functional connectivity, itself is also small. Therefore, it is important to also look at how the variance of COPEs is distributed throughout the brain - if the variance is relatively uniform, it will make more sense to draw conclusions about the strength of the functional connectivity based on the z-stat. Having said this, many literatures establish the link between the strength of the funtional connectivity and the z-stat.

In the resting state experiments, it is common to see that most of the brain (except for the WM and CSF) pass the statistical significance threshold. The left panel of Figure 2-2 shows the pre condition image of the Dexmedetomidine thresholded at the initial z-stat of 2.3. There are two probable explanations for this. First, the BOLD signals are not fully denoised. If there are common noise sources still prevalent in the brain, then correlating the BOLD signals of the two regions would result in spurious correlation and incorrect z-stat. Second, since it is the resting-state, it could be that the ROI has some degree of intrinsic functional connection to many parts of the brain. Between the two, the preferred conclusion would be the latter. Nevertheless, both conclusions emphasizes the importance of the denoising pipeline. It is customary to increase the significance threshold for better visual representation, as in the right panel of Figure 2-2, thresholded at 3.1.

2.1.6 Preprocessing

The preprocessing pipeline has numerous steps - Registration & Normalization of the individual brain to the MNI space, Brain Extraction, Slice Time Correction,

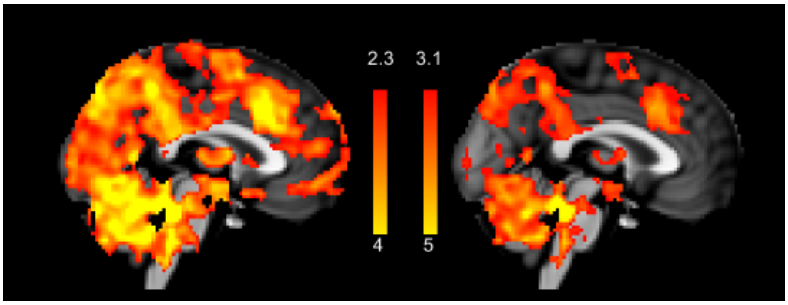

Figure 2-2: Functional Connectivity image of pre condition with Locus Ceruleus seed for different thresholds - 2.3 (left) and 3.1 (right)

Dewarping, and etc. Although equally important, these steps will not be mentioned, as these are widely-accepted standard procedures, common in all variants of the preprocessing pipelines.

Spatial Smoothing

Spatial smoothing is one of the basic steps in the preprocessing pipeline. Spatial smoothing is justified by the fact that spatially adjacent voxels are going to be correlated with each other when activated/deactivated. There are several reasons why spatial smoothing can be beneficial.

1) **Improvement of SNR - Matched filter theorem**: The matched filter theorem states that if the filter matches the underlying signal affected by additive noise, the resulting output of the filter would have the maximum SNR. The spatial smoothing Guassian kernel acts as a filter, in the fMRI context. One could expect that if the width of the kernel matches the underlying voxel activation extent, maximum SNR would be achieved. However, spatial smoothing is usually done independently of the underlying signal, as the extent of the activation is unknown most of the time; in fact, figuring out the spatial extent of activation is one of the main aims of the data analysis. One possible solution would be to iteratively run spatial smoothing with increasing spatial smoothing kernel width to find the optimal width with best SNR. However, this is unfavorable, since it is computationally expensive and the actual activation extent varies across different brain regions.

2) **Accommodation of anatomical and functional variations between subjects**: Even with the sophisticated normalization and the registration algorithms to map individual brains to the standard brain template, certain regions are not going to be mapped to the exact same location in the standard space. This variability can be ameliorated through spatial smoothing, as it blurs together the signals from adjacent areas.

3) **Making the error distributions more normal**: The Central Limit Theorem (CLT) states that the average of the sum of independent Random Variables tends to a normal distribution. The spatial smoothing procedure sums up the noise signals of adjacent voxels, improving the chances of the total noise following a normal distribution, which would satisfy the statistical assumption for inference of parameter estimates, as will be noted in the following sections.

4) **Gaussian Random Field theory**: Gaussian Random Field theory (GRF) is used to solve the multiple comparisons problem in the parametric approach. One of the basic assumptions of GRF is uniform smoothness across the brain. Spatial smoothing thus prepares the data to better satisfy the assumption.

To overcome the limitations of uniform spatial smoothing with the pre-determined kernel width, adaptive spatial smoothing has been proposed recently, which estimates the kernel width locally depending on the data and also uses the adaptive Gaussian Random Field theory to account for non-uniform smoothness [7]. Nevertheless, this procedure is computationally intensive and the resulting improvement in accuracy could be marginal.

The main aim of the spatial smoothing should be the reduction of the individual variability. The degree to which the other potential effects are effective, such as increasing SNR of the data, making the error distribution closer to the normal distribution and smoothing the BOLD data to satisfy the GRF assumption, remains unclear. This is because the underlying signal is noisy and its properties, the spatial extent and smoothness, are hard to estimate. As will be discussed later, the uni-

form spatial smoothing is not always desired, especially for the analyses involving the brainstem, where the conventional kernel width might be too big for brainstem nuclei [8]. The issue of not satisfying GRF can be overcome by using the nonparametric approach, which makes weak distributional assumption about the data.

2.2 General Linear Model & Signal Processing

2.2.1 General Linear Model (GLM)

The General Linear Model (GLM) is a statistical linear model that incorporates a number of different statistical models such as ANOVA, ordinary linear regression, t-test and F-test. The framework is flexible enough that it can be used in multi-level analysis, from the subject level (referred to as 1st-level) to the group level (2nd or 3rd level). This makes GLM a crucial component in fMRI statistical analysis. A canonical form for GLM is given as,

$$Y = X\beta + \varepsilon \tag{2.2}$$

where Y is $N \times 1$ vector, X is a $N \times p$ design matrix with each column corresponding to a regressor, $\beta = [\beta_1, \beta_2, \cdots, \beta_p]^T$ is a $p \times 1$ vector with each element corresponding to a parameter estimate of the corresponding regressor, and ε is the residual error vector. In statistics, Y is referred as a dependent variable and each column of X is referred as an independent variable. In neuroimaging context, Y corresponds to the target signal, such as the BOLD signal of a target voxel. It is easy to see that N is the repetition time, or TR. Design matrix X contains two types of regressors: Regressors of interest and nuisance regressors.

Design matrix regressors

The Regressors of interest refer to the signals for which the parameter estimates are desired, for further statistical analysis. In task-based fMRI, the reference signal obtained from convolving stimulus timeline and the canonical HRF would be the regressor of interest. In the resting state fMRI, BOLD signal extracted from the ROI would be the regressor. The role of the nuisance regressors is to regress out noise from the BOLD data for more accurate parameter estimates of the regressors of interest. These nuisance regressors can include all kinds of signal that the experimenter regards as noise. In fMRI, typical nuisance regressors include motion related regres-

sors, physiological noise, and linear detrending regressor.

1) **Motion regressors**: Head movement is common in fMRI studies, due to respiratory movements or subjects moving slightly out of discomfort. These movements produce motion artifacts in BOLD timeseries and are known to have nonlinear effects on different parts of the brain. To remove the motion artifacts, various motion related regressors are used in the literature. The simplest and the effective way is to include six motion regressors that contain information on how much a subject has moved and rotated between each scan, relative to a reference frame (typically chosen to be the first or the middle scan) in x, y, z direction and around these three axes, respectively. This set of regressors could easily be extended to a set of twelve regressors, by adding temporal derivatives of each of six motion regressors. The additonal temporal derivatives add information of how much the subject has moved at each timeframe relative to the previous one.

2) **Physiological noise regressors**: Physiological noise is one of the most dominant noise sources for mainly two reasons. First, it affects the entire brain. Second, it has been observed that power of the physiological noise is proportional to the fMRI magnetic field, B_0, whereas that of other noise sources, such as thermal noise, is proportional to the square root of B_0 [9]. Physiological noise typically consists of fluctuations due to cardiac and respiratory functions, and is also known to include interaction terms between these processes.

3) **Linear detrending regressor**: The fMRI scanner is known to have linearly increasing magnetic field during the experiment, due to equipment imperfections. This effect is easily accounted for in either of the two ways: By including a linear detrending regressor in the design matrix, or by high pass filtering BOLD timeseries. Since the norm of a regressor is not important for regression, the linear detrending regressor could simply be $x_{linear} = [1, 2, 3, \cdots, N]$. Although the cut-off frequency for high pass filtering depends on the number of scans, the conventional cut-off is $\sim 0.0083\,(Hz)$,

which is equivalent to including a linear detrending regressor for $N = 120$ scans, as $\frac{1}{120} = 0.0083$.

Figuring out better ways to account for the motion artifacts and the physiological noise is an active research topic in the neuroimaging fields, as will be discussed in the following sections. It is interesting to note that, in addition to signal processing and statistical analysis expertise, machine learning algorithms are beginning to be utilized for effective and accurate noise removal.

GLM solutions

Ideally, we want the estimated $\hat{Y} = X\hat{\beta}$ to be as close to Y as possible. The mean squared error, or $E[(Y-\hat{Y})^T(Y-\hat{Y})]$, is the most popular choice for quantifying the closeness of Y and $\hat{Y}$. One of the reasons for popularity is the Gauss-Markov theorem, which will be covered in the following subsection. Another reason is that this error criterion allows for vector representations of the regressors, which brings intuitive interpretation of the regression procedure. For now, let's assume that $Y - \hat{Y} = \varepsilon$ is uncorrelated and have homogeneous variance σ^2 for each TR, or in other words, that the variance-covariance matrix is $\sum = \sigma^2 I$, where I is the identity matrix. Using the least squares method, we can get $c\hat{\beta}$ and $var(c\hat{\beta})$, as follows.

$$\begin{aligned} c\hat{\beta} &= c(X^TX)^{-1}X^TY \\ var(c\hat{\beta}) &= \hat{\sigma}^2 c(X^TX)^{-1}c^T \\ \hat{\sigma}^2 &= \frac{(Y-X\hat{\beta})^T(Y-X\hat{\beta})}{T-p} \end{aligned} \tag{2.3}$$

Since σ^2 is rarely known a-priori, $\hat{\sigma}^2$ is used instead, which is estimated from the data. This estimation results in a tradeoff between the number of regressors, or the Degree of Freedoms (DOF), and the variance $\hat{\sigma}^2$. It might be tempting to include as many nuisance regressors, to account for more possible noise sources in the experiment. However, this is not possible due to the formulation of $\hat{\sigma}^2$. One simple observation is that the number of regressors cannot be more than the number of TRs, since otherwise

$T - p$ and $\hat{\sigma}^2$ will be negative. If adding an additional set of nuisance regressors can account for the unexplained noise variance effectively so that the reduction in the denominator, $(Y - X\hat{\beta})^T(Y - X\hat{\beta})$, can outweigh the reduction in the numerator, $T - p$, it is recommended. However, if the additional set of regressors does not provide much explanatory power, the reduction in $T-p$ due to increased p will result in increased $\hat{\sigma}^2$, contrary to what is desired. Therefore, it is important to carefully examine each individual nuisance regressor's quality and check for the colinearity between them. If there is colinearity between a pair of regressors, meaning that the two regressors are highly correlated, one might be better off including only one of the two regressors, for more DOF.

2.2.2 Temporal Autocorrelation

It is desirable to have the estimated error variance, $\hat{\sigma}^2$, as small as possible. Larger error variance would indicate that the estimate is suboptimal even if it is unbiased. Therefore, if Minimum Variance Unbiased Estimator (MVU Estimator) of β could be found, we could be confident that the resulting $c\hat{\beta}$ is the best estimate possible. Within the GLM framework, the famous Gauss-Markov Theorem states that if the residual errors in the linear regression model are unbiased, uncorrelated, and have homogeneous variances, the least squares estimator is the MVU estimator.

However, in fMRI context, the uncorrelated error assumption is almost always violated. The BOLD signal is autocorrelated, and the resulting residual error is higly likely to be autocorrelated. In this case, the COPE and the variance of the COPE take the following form, for the error variance-covariance matrix $\hat{\sigma}^2 V$:

$$
\begin{aligned}
c\hat{\beta} &= c(X^T V^{-1} X)^{-1} X^T V^{-1} Y \\
var(c\hat{\beta}) &= c(X^T V^{-1} X)^{-1} c^T \hat{\sigma}^2 \\
\hat{\sigma}^2 &= \frac{(Y - X\hat{\beta})^T V^{-1} (Y - X\hat{\beta})}{T - p}
\end{aligned}
\tag{2.4}
$$

This setup, where $V \neq I$, is called the General Least Squares (GLS), as opposed to the Ordinary Least Squares (OLS) where $V = I$. One immediate question is whether there is any assurance that the GLS solution $var(c\hat{\beta})$ is indeed the minimum variance. To answer this, we slightly take a detour and look at the prewhitening method used to mitigate the temporal autocorrelation problem.

Prewhitening method

The autocorrelation in the residual error vector, ε, violates the Gauss-Markov theorem, preventing any conclusion about the minimality of the variance. The prewhitening method aims to solve this by transforming the autocorrelated residual error to an uncorrelated error vector, to satisfy the conditions for the Gauss-Markov theorem. Let K be a matrix that satsifies $KVK^T = I$, where the error variance-covariance matrix is $\sigma^2 V$, as defined previously. We can observe that K is the desired prewhitening matrix:

$$
\begin{aligned}
cov(K\varepsilon) &= E[K\varepsilon\varepsilon^T K^T] \\
&= KE[\varepsilon\varepsilon^T]K^T = \sigma^2 KVK^T = \sigma^2 I
\end{aligned}
\tag{2.5}
$$

Now, we have the following formulation for the GLM:

$$
\begin{aligned}
Y &= X\beta + \varepsilon \\
\Rightarrow KY &= KX\beta + K\varepsilon \\
\Rightarrow Y' &= X'\beta + \varepsilon'
\end{aligned}
\tag{2.6}
$$

Since ε' now satisfies the Gauss-Markov theorem, we have the COPEs and the variance of COPEs as follows:

$$\begin{aligned} c\hat{\beta}_{prewhiten} &= c\left(X'^T X'\right)^{-1} X'Y' \\ &= c\left((KX)^T(KX)\right)^{-1}(KX)^T(KY) \\ &= c\left((KX)^T(KX)\right)^{-1}(KX)^T KXX^T(XX^T)^{-1}Y \\ &= c\left((KX)^T(KX)\right)^{-1}\left((KX)^T(KX)\right)X^T(XX^T)^{-1}Y \\ &= cX^T(XX^T)^{-1}Y \\ &= c(X^TX)^{-1}(X^TX)X^T(XX^T)^{-1}Y \\ &= c(X^TX)^{-1}X^TY \end{aligned} \tag{2.7}$$

$$\begin{aligned} var(c\hat{\beta}_{prewhiten}) &= var(c\left(X'^T X'\right)^{-1} X'Y') \\ &= E\Big[c\left(X'^T X'\right)^{-1} X'Y'\left(c\left(X'^T X'\right)^{-1} X'Y'\right)^T\Big] \\ &= c\left(X'^T X'\right)^{-1} X'E\Big[Y'Y'^T\Big]\left(\left(X'^T X'\right)^{-1} X'\right)^T c^T \\ &= c\left(X'^T X'\right)^{-1} X'KVK^T\left(\left(X'^T X'\right)^{-1} X'\right)^T c^T \\ &= c\left(X'^T X'\right)^{-1} X'\left(\left(X'^T X'\right)^{-1} X'\right)^T c^T \\ &= c\left((KX)^T(KX)\right)^{-1} c^T \end{aligned} \tag{2.8}$$

Due to the Gauss-Markov theorem, $var(c\hat{\beta}_{prewhiten})$ is the minimum variance. One observation is that $c\hat{\beta}$ and $var(c\hat{\beta})$ in (2.4) are the same as $c\hat{\beta}_{prewhiten}$ and $var(c\hat{\beta}_{prewhiten})$ in (2.7) and (2.8). Since they are the same, $var(c\hat{\beta})$ would be the minimum variance.

But how do we estimate V? The discussion so far is based on the assumption that we can estimate V. Estimating the autocorrelation structure based on the data is an active research part, which is out of scope of this work. The widely accepted concept, with regards to fMRI in particular, is that the noise could be modelled with

ARMA(1,1) model, or AR(1) + white noise [10]. This also agrees well with the initial study on exploring the structure of the fMRI noise in the resting state, where the noise was observed to follow $1/f$ structure. More sophisticated approach utilizes band-pass filtering in addition to ARMA models.

All of the previous discussion points to a question of how the temporal autocorrelations at the subject level get propagated to the higher level. Although it is hard to exactly quantify how V affects the outcome, we can use insights from the formulas to make predictions for the group level, as will be discussed in section 2.4 .

2.2.3 Common misconceptions in GLM

Insufficient understanding of the GLM framework often leads to several misinterpretations of the results, which has become quite a problem in neuroimaging literature. In this section, we briefly go over how the linear regression is performed and what the implications are for issues of colinearity, orthgonalization, and other misconceptions in neuroimaging literature.

How Linear Regression is performed

The conventional proof of obtaining parameter estimates $\hat{\beta} = [\hat{\beta}_1, \hat{\beta}_2, \cdots, \hat{\beta}_p]$, which involves partial differentiation to minimize the mean squared error, can obscure the intuitive interpretation of linear regression. Instead, we view it from the geometric perspective, under the name of *Regression by Successive Orthogonalization* [11]. The basic idea is that the parameter estimate $\hat{\beta}_j$ for the jth regressor, $\mathbf{x_j}$, is essentially the same as the regression coefficient for the univariate linear regression of y onto $\mathbf{z_j}$, where $\mathbf{z_j}$ is the result of regressing out other $p-1$ regressors $\mathbf{x_1}, \cdots, \mathbf{x_{j-1}}, \mathbf{x_{j+1}}, \cdots, \mathbf{x_p}$ from $\mathbf{x_j}$. In this case, $\hat{\beta}_j$ would simply be

$$\hat{\beta}_j = \frac{\langle \mathbf{z_j}, \mathbf{y} \rangle}{\langle \mathbf{z_j}, \mathbf{z_j} \rangle} \tag{2.9}$$

The algorithm, which is also known as the Gram-Schmidt prodcedure for multiple regression, could formally be written as follows. For notational convenience, let $\hat{\beta}_p$ be the parameter to be estimated. Then,

1. Initialize $\mathbf{z_0} = \mathbf{x_0} = \mathbf{1}$
2. For $j = 1, 2, \cdots, p$,

   Regress $\mathbf{x_j}$ on $\mathbf{z_0}, \mathbf{z_1}, \cdots, \mathbf{z_{j-1}}$ to get

   1) Coefficients $\hat{\theta}_{kj} = \frac{\langle \mathbf{z_k}, \mathbf{x_j} \rangle}{\langle \mathbf{z_k}, \mathbf{z_k} \rangle}$ for $k = 0, \cdots, j-1$.

   2) Residual vector $\mathbf{z_j} = \mathbf{x_j} - \sum_{\mathbf{k=0}}^{\mathbf{j-1}} \hat{\theta}_{\mathbf{kj}} \mathbf{z_k}$
3. Regress $\mathbf{y}$ onto $\mathbf{z_p}$, to get $\hat{\beta}_j = \frac{\langle \mathbf{z_j}, \mathbf{y} \rangle}{\langle \mathbf{z_j}, \mathbf{z_j} \rangle}$.

Note that $\mathbf{x_p}$ can be any regressor for which we would like to get the parameter estimate of, since the order of the regression is irrelevant. In other words, $\hat{\beta}_j$ represents the unique contribution of $\mathbf{x_j}$ on $\mathbf{y}$, after $\mathbf{x_j}$ has been adjusted for all other regressors $\mathbf{x_0}, \mathbf{x_1}, \cdots, \mathbf{x_{j-1}}, \mathbf{x_{j+1}}, \cdots, \mathbf{x_p}$. This interpretation of multiple linear regression allows us to address common misinterpretations.

Figure 2-3 is a vector diagram that pictorally explains the scheme. Y is the vector representation of the target signal and X_1 and X_2 are the regressors. For simplicity, let's assume that $Y = \beta_1 X_1 + \beta_2 X_2 = X_1 + X_2$, where $\beta_1 = \beta_2 = 1$. b) and c) explain how regression is performed for each regressor. In b), X_2 is regressed against all other regressors, X_1 in this case, resulting in $X_2' = X_2 - \frac{\langle X_2, X_1 \rangle}{\langle X_1, X_1 \rangle} X_1$. Finally, Y is regressed against X_2', which yields $\hat{\beta}_2 = \frac{\langle Y, X_2' \rangle}{\langle X_2', X_2' \rangle} = 1$. The same procedure is applied in c), and the result is $\hat{\beta}_1 = \frac{\langle Y, X_1' \rangle}{\langle X_1', X_1' \rangle} = 1$. The results indicate that $\beta_1 = \hat{\beta}_1 = 1$ and $\beta_2 = \hat{\beta}_2 = 1$, as expected.

Resting state ROI signal

One of the confusions in fMRI arises when extracting the signal from ROI in resting state experiments. Since the ROI signal is used as a reference signal, it can easily be thought that the ROI signal should be fully denoised. Therefore, the nuisance re-

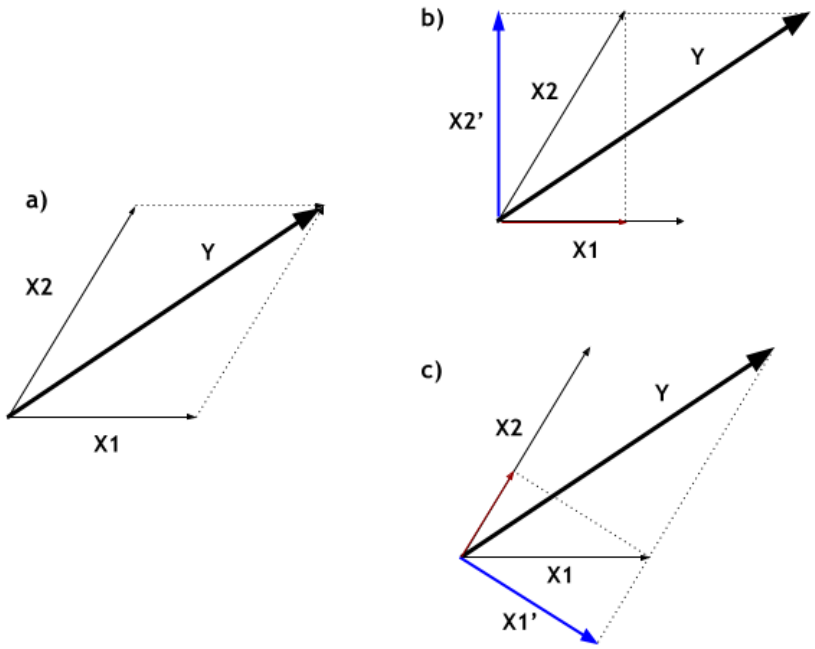

Figure 2-3: Regression scheme for *Regression by Successive Orthogonalization*

gressors would have to be regressed out from the brain prior to the extraction of the ROI signal. However, we can see that this is not necessary, if we are interested only in $\hat{\beta}_{ROI}$. Even if the ROI signal contains various noise components, the parameter estimate for the ROI signal, $\hat{\beta}_{ROI}$, would only represent the contribution of $\mathbf{x_{ROI}}$ adjusted to all other regressors, the nuisance regressors. In other words, if the nusiance regressors are correctly set up, $\hat{\beta}_{ROI}$ would only be relevant to the neuronal BOLD signal of the ROI, as desired.

Figure 2-4 is a vector diagram with the same vectors as in Figure 2-3. Without loss of generality, let us assume that X_1 is the nuisance regressor and X_2 is the regressor of interest. The first step, depicted in b), is to regress Y against X_1, which returns the residual vector $R_1 = Y - X_1' = Y - \frac{\langle Y,X_1\rangle}{\langle X_1,X_1\rangle}X_1$ and $\hat{\beta}_1 = \frac{\langle Y,X_1\rangle}{\langle X_1,X_1\rangle} > 1$. One important point is that X_2 is also regressed against X_1 in the process, as the scheme is to regress X_1 against the entire brain signal, meaning that X_2, the ROI signal, is also affected. The regression yields $X_2' = X_2 - \frac{\langle X_2,X_1\rangle}{\langle X_1,X_1\rangle}X_1$. The next step, depicted in c), is essentially regressing $R_1 = Y - X_1'$ against X_2'. It is easy to see that $R_1 = X_2'$, yielding

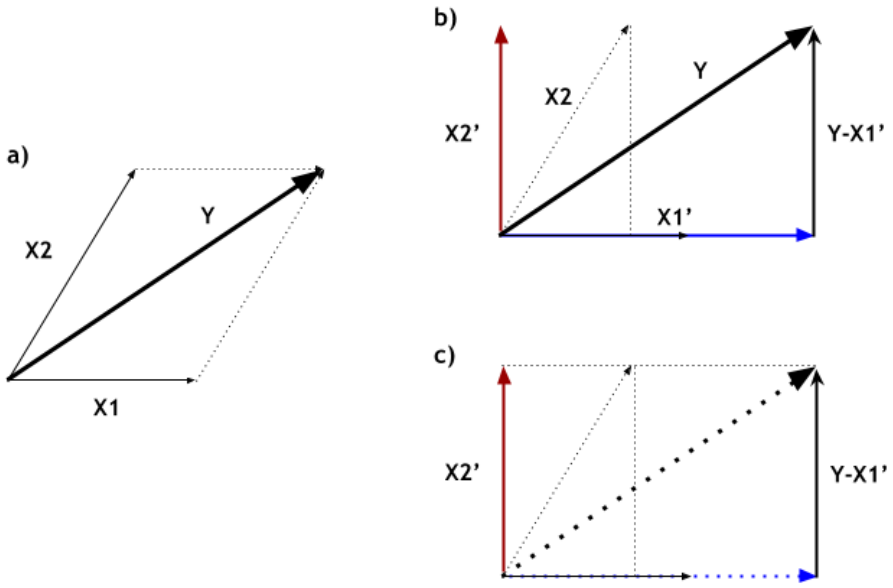

Figure 2-4: Regression scheme which regresses out the nuisance regressors (regressors of no interest) first

$\hat{\beta}_2 = 1$. Although $\hat{\beta}_1$ is different from that of the previous example, it is important to observe that $\hat{\beta}_2$ is the same. This is because from the X_2 perspective, the procedures to obtain $\hat{\beta}_2$ are the same in both cases. $\hat{\beta}_1$ is increased in this example, as the shared variability between X_1 and X_2, which is the noise, is soaked up into X_1. Since we are only interested in the parameter estimate for the regressor of interest, $\hat{\beta}_2$, the value of $\hat{\beta}_1$ is irrelevant. In general, the COPE, $c\hat{\beta}$, would be the same in these two approaches. This has important implication for manually orthogonalizing regressors, which will be discussed in the following section.

There are indeed cases when noise-free ROI signal is desired and hence nuisance factors need to be regressed out from the brain first. If the intention is to examine the Pearson correlation measure between the ROI signal and the BOLD signal of a target voxel, one would want the reference ROI signal and the target voxel signal to be as uncontaminated as possible. This approach is used frequently in the studies of correlated/anti-correlated networks of the resting state brain [12]. If this approach is to be used for further group analysis, one needs to be careful when calculating the

variance of the COPEs. In this case, the design matrix would only contain the ROI signal, which might falsely lead the user (or the program) to assume that the Degree of Freedom is $T-1$, when in fact it is $T-p$. This would result in smaller variance of the COPEs, and increased test statistics, yielding higher number of false positives.

Orthogonal regressors

Another misinterpretation in the neuroimaging literature is that the orthogonalization of regressors is recommended to avoid colinearity between the regressors. In popular fMRI softwares, such as SPM and FSL, there are options to orthogonolize the regressors. To see why orthogonalization might lead to misinterpretation, let's think of two cases: 1) Orthogonalize all other regressors with respect to $\mathbf{x}_{ROI}$. 2) Orthogonalize $\mathbf{x}_{ROI}$ with respect to all other regressors.

In the first case, it is true that the ROI signal is now uncorrelated to the other orthogonalized nuisance regressors. However, this means that the shared variability between the ROI signal and other nuisance regressors, which caused the correlations between the signals in the first place, would be fully soaked up by the ROI signal. Thus, the orthogonalized nuisance regressors would not be able to denoise the ROI signal. $\hat{\beta}_{ROI}$ would then indicate the regression coefficient for *the ROI signal + noise signal in the ROI*, instead of *the ROI signal denoised with the nuisance regressors*, which is not the desired estimate.

In the second case, the resulting ROI signal is indeed noise-free and thus its shared variability with other regressors would have been soaked in by others. $\hat{\beta}_{ROI}$ would now represent the desired quantity. Nevertheless, this is exactly what would be obtained through the Gram Schmidt procedure. Therefore, orthogonalization is redundant in this case.

It is important to realize that regardless of which regressor the rest of the regressors are orthogonalized against, the overall prediction, $\hat{\mathbf{Y}} = X\hat{\beta}$ will be the same,

although $\mathbf{X}$ and $\hat{\beta}$ will change according to the orthogonalization scheme. Different orthogonalization schemes simply correspond to different ways to assign shared variabilities among different parameter estimates, $\hat{\beta}_i$s. If the goal of the linear regression is to find the best estimate of the dependent variable $\hat{\mathbf{Y}}$, then orthogonalization is not required at all. However, if the goal is to get the parameter estimate for some regressor $\hat{\beta}_i$, different orthgonalization schemes would produce different estimate. Thus, orthgonalization is not recommended, unless there is a strong argument for it.

Nuisance regressors

Other than the motion regressors, which are derived from the external measurements, the nuisance regressors are extracted from the noise ROIs such as Cereberal Spinal Fluid (CSF) and White Matter (WM). It is important to ensure that these regions are unlikely to include neuronal BOLD signals from the adjacent Gray Matter regions. If there is a contamination, the estimation of $\hat{\beta}_{ROI}$ will be less accurate. With other regressors containing parts of $\mathbf{x}_{ROI}$, the unique contribution of $\mathbf{x}_{ROI}$ on $\mathbf{Y}$ adjusted to other regressors would be misrepresented, due to other regressors containing parts of $\mathbf{x}_{ROI}$. Recall that the reciprocal contamination, nuisance signals included in the ROI signal, is not as serious, since the noise would be taken into account when $\mathbf{x}_{ROI}$ is computed.

This is why extra care must be put into defining the noise ROI masks. If the masks include the voxels on the boundary regions of WM and GM, or CSF and GM, it is likely that the neuronal signals would be present in these voxels after spatial smoothing. There are several ways to mitigate this. The simplest and common procedure is to erode the noise ROI masks to ensure that the confounding voxels are not included. Another possibility is to extract nuisance signal from unsmoothed noise ROI. This is particularly effective when the noise ROI is so small, such as the 4th ventricle region, that erosion of the mask is unfavorable.

2.2.4 White & Gaussian Noise

One important class of concepts that are often misunderstood is Gaussian noise and White noise. Gaussian noise is concerned with the amplitude of the noise at the given point, assuming that the noise amplitude is sampled from the Gaussian distribution. Gaussian noise in neuroimaging literature is important mainly for two reasons. First, due to the Central Limit Theorem (CLT), the sum of many independent noise sources can be treated as having a Gaussian Distribution. Since it is impossible to account for all possible noise sources affecting the signal, the remaining noise sources after removing physiological, movement, and scanner noise are treated as a single noise source following the Gaussian distribution. As it is reasonable to assume that there are many unaccounted independent noise sources, the Central Limit Theorem provides the justification for the Gaussian noise. The second importance arises in parametric model context, which will be addressed in later sections.

On the other hand, the white noise is about the temporal characteristic of the noise, and states that the noise is temporally uncorrelated with itself. It is best characterized by its power spectrum being flat throughout the whole frequency (or to be more precise, within the bandwidth of interest). Its importance arises in the parametric model context, as with the Gaussian noise. The parametric approach is predicated on the assumption that the test statstic follows a certain parametric distribution, namely the t-distribution. For this assumption to hold, the residual error, or the residual noise after regression, needs to be normally distributed and temporally uncorrelated, or in other terms, needs to be Gaussian White noise.

The common confusion between the two different terms leads to these being used interchangeably. For instance, the measurements of fMRI scanner noise indicate that the noise spectra is flat enough, that it can be approximated as a white noise [13]. However, this is not an indication that the scanner noise is a Gaussian noise.

2.2.5 Physiological Noise Correction

There are several ways to remove the physiological noise which, along with the movement artifacts, confounds the outcome. Although different, the majority of the denoising methods are based on a common observation that the noise ROIs are unlikely to contain any neuronal signals. Therefore, whatever BOLD signal is captured in these regions, it is very likely that it is an aggregate of noises from several independent sources, such as cardiac, respiratory response, thermal noise, and even head movements. It is certainly possible for the BOLD signal in noise ROIs, especially on the boundaries, to contain some neuronal signals leaked from the neighboring Gray Matter (GM). For this reason, it is important to run physiological noise correction procedures only on the subregions of noise ROIs not close enough to GM.

Averaged WM/CSF regressors

This is the simplest method for removing the physiological noise. As the name suggests, the nuisance regressors are obtained from averaging BOLD signals of all the voxels in the noise ROIs. Usually, one is obtained from WM region and the other from CSF region, thus producing two nuisance regressors in total. These regressors are shown to capture the representative noise in each ROI relatively well without reducing DOF by much (in this case, only two DOF reduction). Also, due to simple implementation, this method has been dominant for a few decades.

The biggest weakness of the method is that it collapses different BOLD signals from thousands of voxels into one averaged signal. This would work fine if the BOLD signals in the noise ROIs are in phase, which is rarely the case, due to the nonlinear effects of physiological noise and motion. If not, this would lead to constructive/destructive interference when averaging the signals, producing ineffective nuisance regressors.

Bandpass Filtering

Since the cardiac and respiratory movements are quite regular throughout the experiment, the spectrum of BOLD signal affected by the physiological noise would ideally have two peaks, corresponding each to cardiac and respiratory source. In this case, these signals could be bandpass filtered, producing the physiological noise free BOLD signal. However, this approach is infeasible, as the usual TR value (2$\sim$3 seconds) results in low Nyquist frequency, much lower than where the physiological noises are expected to exist. As a result, the physiological noises are aliased to lower frequencies. This is compounded by the fact that there are overwhelming evidences that the resting state brain maintains its functional connectivity between the regions using low-frequency signals ($\sim$ 0.1 Hz). As such, bandpassing the suspected frequency band to remove the phsyiological noise in the low frequency is also likely to remove the signal of interest. Moreover, recent studies show that there are interactions between the cardiac and respiratory systems, such as increased cardiac output during inspiration (respiratory pump) and changes in CSF flow, which are observed to lie in different frequency bands other than cardiac and respiratory signals [14]. The interactive term further complicates the bandpass filtering procedure.

CompCor (Component-based Correction)

CompCor uses Principal Component Analysis (PCA) to extract more information than just the averaged signal from the noise ROIs [15]. PCA is used on the variance-convariance matrix of the noise ROI data to calculate eigenvalues and the corresponding eigenvectors. Typically, five eigenvectors (Principal Components) with the biggest eigenvalues are included as the nuisance regressors. With the five regressors each from CSF and WM, this amounts to ten physiological nuisance regressors.
Previous results show that these principal component regressors show similar performance in capturing respiratory and cardiac signals, compared to the RETROICOR. In addition, the method has also been shown to regress out nonlinearity caused by the motion artifacts reasonably well.

The previous works on CompCor does not attempt to explain why the noise ROI principal components are effective in capturing the noise signal. Explaining the effectiveness of PCA is one of the main focus of the thesis.

RETROICOR

The RETROICOR method utilizes physiological recording to subtract the physiological noise from fMRI signal [16]. Photoplethysmogram is used to monitor the cardiac cycles and pneumatic belt is used to capture the respiratory cycles. These information are used to construct low order Fourier series to represent the physiological signals. Despite its simplicity, RETROICOR has maintained its status as the most effective method to account for the physiological noise, should the monitoring tools be available throughout the experiment.

2.3 Multiple Comparisons

The multiple comparisons problem arises as there are too many hypothesis tests to be performed within a single image, as many as the number of voxels in the image, if the tests are voxel-based. Even if we assume that every voxel response follows the null distribution, if the significance threshold is α, there will be $(number\ of\ voxels) \times \alpha$ false positive (Type I Error) voxels by chance. This is troublesome, when there are activated voxels, as it would be difficult to distinguish the voxels from the false positive voxels. The multiple comparisons problem arises in numerous different contexts, and thus has occupied interests of many statisticians over the past decades. Among several measures, Family-wise error rate (FWER) is the most widely used measure and thus will be the central focus of the section.

In fMRI context, there are two important aspects to consider. The first is the basic unit on which the hypothesis testing is performed. The unit could be each individual voxel in the image, which requires as many tests as the number of voxels in the image. The unit could also be a cluster formed by adjacent suprathreshold voxels (the threshold is manually defined), which requires much less tests than the voxel case, but requires sophisticated mathematics for analysis. The second aspect is choosing between the parametric and non-parametric approach. The aim of this section is to explore how the hypothesis tests for both cases are dealt with, in both the parametric and non-parametric contexts.

2.3.1 Family-wise error rate (FWER)

The conventional p-value α will result in non-trivial number of false positives when there are many multiple comparison tests to be done. Therefore, α needs to be readjusted to exhibit tighter control over the number of false positive voxels or clusters. Family-wise error rate (FWER), α_E, controls the probability of there being at least one false positive result in the entire family of hypothesis tests. In fMRI context, the family of tests would refer to the collection of hypothesis tests carried out the

whole brain. It is a very stringent measure, especially for a voxel case, since out of 10^6 voxels, we are controlling the probability of there being at least one false positive voxel to be low, typically 0.05. As can be seen in following subsections, as a result of the stricter control over the entire family, the adjusted individual p-value α will become really small, resulting in high significance threshold. For example, let $FWER = \alpha_E = 0.05$ and there are 10^6 voxels in the brain. The adjusted α or the corrected p-value would now be $\alpha = 5 \times 10^{-8}$, which is much stricter than the usual $\alpha = 0.05$.

2.3.2 Voxel test

Parametric approach - Sidak Correction & Bonferroni Correction

Putting the fMRI context aside for a bit, let's assume that there are m independent hypothesis tests in the family and we want to control FWER, α_E, by adjusting the individual voxel hypothesis threshold α. Notice that

$$\begin{aligned} P(FWER) = \alpha_E &= P(\textit{At least 1 FP in the Family}) \\ &= 1 - P(0\ \textit{FP in the Family}) \end{aligned} \tag{2.10}$$

Note that Sidak Correction is concerned with the omnibus null hypothesis, where all the data are assumed to be drawn from null distribution and thus there are m number of null hypothesis beinging tested. Since the probbility that a single voxel drawn from the null distribution is not false positive is $1-\alpha$, or $P(\textit{the voxel is not FP}) = 1-\alpha$, we have

$$\begin{aligned} &P(FWER) = \alpha_E = 1 - (1-\alpha)^m \\ &\Rightarrow (1-\alpha)^m = 1 - \alpha_E \\ &\Rightarrow \alpha = 1 - (1-\alpha_E)^{\frac{1}{m}} \end{aligned} \tag{2.11}$$

Obviously, this is only one of numerous possibilities, as some voxels are bound to have true signal that are not from null distributions. In these voxels, $P(\textit{the voxel is not } FP) = 1$, since these voxels cannot be false positives. To control for the case in which only m_0 voxels out of m voxels are from the null distribution,

$$\begin{aligned} &\alpha_E = 1 - P(0\ FP\ \textit{in the Family}) = 1 - (1-\alpha')^{m_0} \\ &\Rightarrow \alpha' = 1 - (1-\alpha_E)^{\frac{1}{m_0}} \geq \alpha = 1 - (1-\alpha_E)^{\frac{1}{m}} \end{aligned} \tag{2.12}$$

Since $\alpha' \geq \alpha$, and thus the significant threshold for α' is lower than that for α, we have less strict control as a result of knowing m_0. This is nearly impossible, as we do not know exactly how many voxels are going to be from null distribution before running the experiment. Nevertheless, what we do know is that regardless of the value of m_0, $\alpha' \geq \alpha$ always holds. No matter what the actual number of "true" voxels is in the image (from 0 to all voxels in the image), setting the adjusted p-vlaue to be α, calculated assuming that every voxel is drawn from the null distribution, ensures that the FWER will be kept below α_E. This is why the Sidak Correction is termed as a *strong contro*l of FWER.

This is a parametric approach, as the p-value is converted to the corresponding significance threshold according to the parametric null distribution, which most likely would be the z distribution. The voxels that pass this threshold can be treated statistically significant, adjusted for multiple comparisons.

However, the Sidak correction is not as practical in fMRI context. The basic assumption of the Sidak Correction is that the tests need to be independent of each other. However, the tests in voxels cannot be independent, especially if the voxels are close to each other, for various reasons. First, an activated brain region already implies that the voxels in the region are activated/deactivated together, not independent from each other. Second, due to the several procedures in preprocessing, especially spatial smoothing, the BOLD signals in the voxels are bound to be correlated with

each other to some degree. This makes it hard to determine the number of independent hypothesis tests, which is the fundamental assumption of the Sidak Correction. This is why the multiple comparisons solutions for clusters are preferred over those for the voxels. Having stated this, lots of literature still use the Sidak correction in the form of voxel-wise correction.

Non-parametric approach

The basic idea of the nonparametric approach is to minimize the distributional assumptions about the data, by constructing the reference null distribution from the given data. Recall that in the parametric approaches, parametric distributions such as t-distribution and χ^2 distribution were used as the reference null distribution. The main idea for the nonparametric approach is that if the data are sampled from the null distribution, even if the data are shuffled, the newly computed test statistic for the shuffled data would still be statistically insignificant.

Another important advantage of the nonparametric approach is that the test statistic does not have to be standard, meaning that closed mathematical form needs not exist. In imaging context, this can range from the standard t-statistic or cluster size, to the non-standard statistic such as cluster-mass, pseudo t-statistic, and threshold-free cluster enhancement statistic. The only requirement is that these quantities be pivotal statistics [18].

It is important to define how the test statistics are to be computed for each iteration, or more explicitly, how the existing data is going to be exploited. The most dominant procedure in the field is randomize, or shuffling, the existing data - it is hard to find works using Bootstrapping, also a very popular framework in general nonparametric context, in neuroimaging studies. In the single subject context, the BOLD signals across TRs within each voxel are shuffled to produce new test statistic for each iteration. This is a reasonable choice, as the new test statistic of the shuffled data should not be statistically significant, if the voxel were in the null con-

dition. These test statistics, collected from entire iteration, are used to construct the null distribution from which the significance threshold corresponding to the desired FWER is calculated.

This is where the confusion arises. Should the null distribution be constructed for each individual voxel, using the test statistics gathered only from that voxel? In this case, the statistical significance of a voxel will be decided on the basis of the specifc null distribution for the voxel. However, this is incorrect since the multiple comparisons problem is not solved - the hypothesis tests will still be performed as many times as the number of voxels. This method brings us back to ground zero.

Now, the question remains as to how the test statistic in each voxel and iteration is used in the whole brain image. This extension from the single voxel to the whole image requires an additional concept, namely the max distribution. Since the family-wise error rate controls the probability that there is at least one false positive voxel in the image, the idea is to only look at the maximum statistic in the entire image. If this maximum statistic does not exceed the significance threshold, then none of the other voxels within the image would cross this threshold. Therefore, the probability that the maximum statistic crosses the threshold under the null hypothesis is equivalent to the probability that at least one voxel is false positive under the null hypothesis, namely the FWER.

$$P(FWER) = P(At\ least\ one\ voxel\ false\ positive \mid H_0) = P(Max\ statistic > threshold \mid H_0) \tag{2.13}$$

The procedure is to keep track of the max statistic value across the image for each iteration and construct the null reference distribution from these values. Then, the test statistics of the original image would be compared against the significance threshold from the null reference distribution to determine the significance.

On the side note, it is important to note that the non-parametric approach also

suffers from the temporal autocorrelation in the BOLD signal. The crucial assumption for being able to shuffle the data is that it is inherently exchangeable, which is hard to guarantee in the presence of the temporal autocorrelation. This has led to numerous studies on exchangeability of data in general and how to perform nonparametric approaches even if the assumption is violated. As will be discussed in the later section, this is not so much of a problem at the group level, since the COPEs are shuffled within the restricted exchangeable blocks, not the BOLD signals within each voxel.

2.3.3 Cluster test

The alternative to the voxel-based approach is the cluster-based approach. This requires significantly less number of hypothesis tests, since the number of clusters is going to be much less than the number of voxels. It is interesting to note that the number of tests for the cluster-based approach itself is a random variable, since the number of clusters is not a fixed quantity. This is in contrast with the voxel-based approach, where the number of the test are fixed (unless some pre-masking is done), as the number of voxels are fixed. There are mainly two test statistic for the cluster-based approach: 1) cluster size and 2) cluster size and height. Among these two metrics, cluster size is generally preferred, due to its relative simplicity.

Parametric approach - Gaussian Random Field Theory

The Gaussian Random Field Theory is a parametric approach that constructs an overall joint null reference distribution for the voxels in the image. More specifically, the theory assumes that under the null reference hypothesis, the voxels in the image are jointly distributed under a multivariate normal distribution, with some amount of spatial correlation between the neighboring voxels. If the spatial correlation within the image is known, it would be possible to calculate a significance threshold of the cluster size, similar to α in the Sidak correction, which also depends on the desired FWER. The spatial correlation within the image, or the amount of smoothness, is

termed as the resolution units (RESELs) in the context of GRF, and is the most fundamental quantity that needs to be calculated for the application of GRF for fMRI multiple comparisons problem. If the assumptions of GRF are satisfied, the threshold for the cluster size can be analytically derived, as a function of RESELs and FWER in 2D and 3D [17]. These solutions are used frequently by the fMRI processing softwares for parametric approaches, such as FSL and SPM.

Nonparametric approach

There are several steps to the nonparametric cluster approach. For each iteration, shuffling within the voxel (same as the procedure in the nonparametric voxel test) is performed to calculate z-stat for each voxel. After the caculation is done for the whole brain, the conventional z-stat threshold of choice (normally 2.3 or higher) is applied. Among the clusters formed by the thresholding process, the largest cluster's size is recorded for constructing the max distribution. These steps are repeated for the number of iterations. For the cluster approach, eq 2.13 is slightly modified as the following,

$$\begin{aligned} P(FWER) &= P(At\ least\ one\ clusterl\ false\ positive \mid H_0) \\ &= P(Max\ cluster\ size > size\ threshold \mid H_0) \end{aligned} \tag{2.14}$$

Only the clusters that pass the threshold corresponding to the FWER in the max distribution, are deemed statistically significant.

2.3.4 Application in pre-masked regions

So far, the image in the multiple comparison discussion meant the whole brain, encompassing $\sim 10^6$ voxels (in MNI space with 2mm isotropic voxel). Ensuring FWER of 0.05 on this sheer number of voxels could result in stringent significance thresholds, which is not desirable in some cases. One popular solution is to simply reduce the size of the image, by restricting the mask to certain regions of the brain that are likely to be significant. Since the number of the required tests is reduced, the significance

threshold is also lowered, possibly showing more activated voxels/clusters. In the parametric approach, this is reflected in the equations yielding lower threshold due to the reduced number of voxels (Sidak Correction) and RESELS (GRF), respectively.

In the nonparametric approach, we can arrive at the similar conclusion as follows. For the ith iteration, let $t_{i,whole}$ be the max test statistic of interest (i.e. cluster size) in the whole brain. Let $t_{i,masked}$ be the equivalent counterpart in case of the masked brain. We can easily see that $t_{i,whole} \geq t_{i,masked}$ always holds. If this does not hold, such that for some iteration j, $t_{j,whole} < t_{j,masked}$, it is a contradiction since $t_{j,whole}$ is defined to be the max test-statistic in the whole brain, and the masked region is a subset of the whole brain. As a result, it is also straightforward to see that $\alpha_{whole} \geq \alpha_{mask}$, or in other words the significance threshold for the whole brain is greater than or equal to that for the masked brain, since the null distributions are constructed from $\{t_{i,whole}\}$ and $\{t_{i,masked}\}$, respectively. A simple example is shown in Figure 2-5. Since α, the original test-statistic p-value for ROI, is greater than α_{mask}, but smaller than α_{whole}, the ROI will be statistically significant in the masked analysis, but insignificant in the whole-brain analysis.

The effectiveness of the pre-masking procedure depends on how much the threshold is reduced - If the lowered threshold is still higher than the test statstics of the ROIs, these regions will still be statistically insignificant. Moreover, one needs to make sure that the mask is well-defined, so that it does not leave out any potentially significant regions.

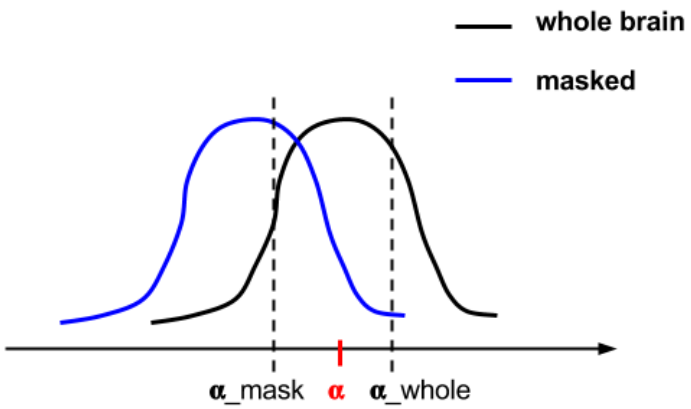

Figure 2-5: The shifted Max-statistic distribution of the test statistic of interest. α_{whole} and α_{masked} are the signficance thresholds of the unmasked and masked brain, respectively. α is the original test statistic of ROI. The two null distributions are not necessarily the same shape.

2.4 Group-Level Inference

After the parameter estimation at the subject level, the estimates are passed onto the higher level for inference on a group or whole population from which these subjects were selected. Since the neuroimaging experiments can never be run on the entire population, one must rely on statistical techniques to carefully extend the results from the sampled group (usually $N < 100$) to the general population. There are two major ways for group-level inference, the fixed model and the mixed model.

One must first understand the concept of fixed and random factors. For a given set of experiments, any factor that is used in repetition throughout the experiments are called fixed factors [19]. For example, if a study wants to investigate the levels of unconsciousness caused by a certain anesthetic drug on different age groups, the drug would be treated as a fixed factor. These factors are chosen carefully for their specific properties. On the other hand, if certain factors are not fixed and randomly sampled for each experiment, these are called random factors. Subjects are usually the random factors, since the subjects recruited for a specific study are almost never the same subjects, and thus could be treated as having been sampled randomly from the whole population. However, it must be noted that there are studies where the

subjects are fixed factors. For example, experiments that are run on patients with neurophysiological disorders due to their uniqueness, are likely to use the same set of subjects repeatedly.

Parameter estimations on the fixed factors are limited in a sense that the parameters provide little to no information regarding the other factors. For example, if a certain anesthesic drug is used as a fixed factor, the estimate from the study does not provide any information on other types of the drugs. This makes the fixed factors unfavorable for generalization to bigger groups which these are part of. Nevertheless, estimation is more accurate when a factor is fixed rather than random, for the reasons we will soon address. On the other hand, the random factors enable the estimation to be generalized to the broader category.

In the following subsections, we will focus on how treating the subjects as fixed or random factors produce different results and what the implications would be in terms of resource allocation.

2.4.1 GLM at the higher level

At higher levels, the objective of the inference is whether the group average effect size has any statistical significance. The inference is based on the individual effect size, calculated from the subject-level. Therefore, the design matrix takes a different form, with each row representing either a session or subject effect size, instead of a voxel intensity at a specific TR. It is convenient to regard each element of the design matrix as an indicator variable, with 1 representing that the subject/session is indeed in the group and 0 otherwise.

$$\begin{aligned} Y_i &= X_i\beta_i + \varepsilon_i \\ \beta_i &= \beta_G + \varepsilon_{G,i} \\ \Rightarrow Y_i &= X_i\beta_G + X_i\varepsilon_{G,i} + \varepsilon_i \end{aligned} \tag{2.15}$$

Depending on what the focus of the experiment is, the design matrix setup is different. We briefly look at the three most common cases and how the design matrix is set up in each of these scenarios.

Group average effect - one sample t-test

This is the simplest case in which the aim is to test whether the group average effect size, which is $\beta_G = \frac{1}{N}\sum_{i=1}^{N}\beta_i$, is statistically different from 0. Therefore, the null hypothesis would be $H_0 : \beta_G = 0$. The design matrix would simply be a column of 1s, size of $N \times 1$.

Difference between group average effect - two sample t-test

The aim is to test whether the effect size of group A, with N_1 subjects, is significantly different from that of group B, with N_2 subjects. This is mostly the case when there is a control group and an experiment group, and the subjects in either groups are not necessarily the same. Let $\beta_{G,1} = \frac{1}{N_1}\sum_{i=1}^{N_1}\beta_i$ and $\beta_{G,2} = \frac{1}{N_2}\sum_{i=1}^{N_2}\beta_i$ be the group average effect size for group 1 and 2, respectively. Then, the null hypothesis would be $H_0 : \hat{\beta}_{G,1} - \hat{\beta}_{G,2} = 0$, and the design matrix would be of the following form:

$$X = \begin{pmatrix} 1 & 0 \\ \vdots & \vdots \\ 1 & 0 \\ 0 & 1 \\ \vdots & \vdots \\ 0 & 1 \end{pmatrix}, \quad \beta_G = \begin{pmatrix} \beta_{G,1} \\ \beta_{G,2} \end{pmatrix} \tag{2.16}$$

, where X is $(N_1 + N_2) \times 2$ matrix.

Difference between group average effect - paired t-test

The aim is same as the two sample t-test. The only difference is that the subjects in the both group are the same, and the measurements are taken at two different

conditions. The design matrix would be of the following form:

$$X = \begin{pmatrix} 1 & 1 & 0 & \cdots & 0 \\ 1 & 0 & 1 & \cdots & 0 \\ \vdots & & & & \\ 1 & 0 & 0 & \cdots & 1 \\ -1 & 1 & 0 & \cdots & 0 \\ -1 & 0 & 1 & \cdots & 0 \\ \vdots & & & & \\ -1 & 0 & 0 & \cdots & 1 \end{pmatrix}, \quad \beta_G = \begin{pmatrix} \beta_{G,1} \\ \beta_2 \\ \vdots \\ \beta_{N+1} \end{pmatrix} \tag{2.17}$$

where X is a $2N \times (N+1)$ matrix, where N is the group size. ith row and $(N+i)$th row would correspond to the subject i, where $1 \leq i \leq N$. $\beta_{G,1}$ is the parameter estimate of the effect size difference between the two conditions within each individual, whereas β_i, where $2 \leq i \leq N+1$ is the dummy parameter to regress out any *mean effect* of the $(i-1)$th individual. The null hypothesis would be $H_0 : \hat{\beta}_{G,1} = 0$, meaning that the group difference is not significant. It is easy to see that the effect size difference for subject i, $Y_{i,A} - Y_{i,B}$ is $2\beta_{G,1}$. β_2, β_3, and β_4 are for modeling the average effect size for each subject and have no statistical meaning and therefore, is irrelevant to the hypothesis. It is important to acknowledge that each of these parameters capture what is common between the two conditions within each subject, such as age (assuming that these measurements were taken within few weeks of each other) and gender.

two sample t-test vs. paired t-test

Since the two sample and the paired t-test both aim to compare the group average effect between the two groups, both are eligible for the Dexmedetomidine study. Nevertheless, the paired t-test is preferred, as the individuals in the two groups are the exactly the same. A simple example will help us understand why. Suppose $N = 3$ (Female 30 years old, Male 40 years old, Female 55 years old), and we wish to test whether there is any significant difference in the effect size for condition A and

condition B. Then, the GLM in the two-sample t test case will be

$$\begin{pmatrix} Y_{1,A} \\ Y_{2,A} \\ Y_{3,A} \\ Y_{1,B} \\ Y_{2,B} \\ Y_{3,B} \end{pmatrix} = \begin{pmatrix} 1 & 0 & 1 & 30 \\ 1 & 0 & 0 & 40 \\ 1 & 0 & 1 & 55 \\ 0 & 1 & 1 & 30 \\ 0 & 1 & 0 & 40 \\ 0 & 1 & 1 & 55 \end{pmatrix} \begin{pmatrix} \beta_1 \\ \beta_2 \\ \beta_{sex} \\ \beta_{age} \end{pmatrix} + \varepsilon = \begin{pmatrix} \beta_1 + \beta_{sex} + 30\beta_{age} \\ \beta_1 + 40\beta_{age} \\ \beta_1 + \beta_{sex} + 55\beta_{age} \\ \beta_2 + \beta_{sex} + 30\beta_{age} \\ \beta_2 + 40\beta_{age} \\ \beta_2 + \beta_{sex} + 55\beta_{age} \end{pmatrix} + \varepsilon \tag{2.18}$$

The GLM in the paired t-test case will be

$$\begin{pmatrix} Y_{1,A} \\ Y_{2,A} \\ Y_{3,A} \\ Y_{1,B} \\ Y_{2,B} \\ Y_{3,B} \end{pmatrix} = \begin{pmatrix} 1 & 1 & 0 & 0 & 1 & 30 \\ 1 & 0 & 1 & 0 & 0 & 40 \\ 1 & 0 & 0 & 1 & 1 & 55 \\ -1 & 1 & 0 & 0 & 1 & 30 \\ -1 & 0 & 1 & 0 & 0 & 40 \\ -1 & 0 & 0 & 1 & 1 & 55 \end{pmatrix} \begin{pmatrix} \beta_1 \\ \beta_2 \\ \beta_3 \\ \beta_4 \\ \beta_{sex} \\ \beta_{age} \end{pmatrix} + \varepsilon = \begin{pmatrix} \beta_1 + \beta_2 + \beta_{sex} + 30\beta_{age} \\ \beta_1 + \beta_3 + 40\beta_{age} \\ \beta_1 + \beta_4 + \beta_{sex} + 55\beta_{age} \\ -\beta_1 + \beta_2 + \beta_{sex} + 30\beta_{age} \\ -\beta_1 + \beta_3 + 40\beta_{age} \\ -\beta_1 + \beta_4 + \beta_{sex} + 55\beta_{age} \end{pmatrix} + \varepsilon$$

(2.19)

The difference between (2.18) and (2.19) is the existence of the mean effect parameter. Note that in the paired t-test, the age & sex effects can be absorbed into $\beta_2 \sim \beta_4$ (for example, $\beta_2' = \beta_2 + \beta_{sex} + 30\beta_{age}$), as we are only interested in the difference between the two conditions, β_1, not the absolute value of the effect size. Even if there are some unaccounted effects that might cause individual variability, the mean parameters would automatically take care of these. However, in (2.18), these factors need to be explicitly modelled due to the absence of the mean parameters. Otherwise, the unaccounted variability would be absorbed into $\hat{\beta}_1$ and $\hat{\beta}_2$, the group average parameter estimates, and affect the outcome of the test.

For these reasons, if the control and the experiment group are the same, the paired t-test is always preferred over the two-sample t-test - It is more efficient as the number of required subjects to make statistical conclusion is smaller in the two-sample t-test. Nevertheless, if the control and experiment group are of different individuals, which is a very common situation, the paired t-test cannot be applied and the two-sample t-test should be used.

2.4.2 Summary Statistic approach

For group-level analysis, inference results for each individual subject are required. It has been shown that only the COPEs and the variance of COPEs are required from the subject level, a method termed as the summary statistics approach [20]. This approach saves great deal of computation power, as not all the information, such as design matrix, has to be passed on to the group level from the subject level. In fact, only one group-level inference method requires both the information on COPEs and the variance of COPES. As for the other parametric method and the nonparametric method, only the COPEs are required.

Parametric approach - Fixed model

For the fixed model, we assume that the subjects are fixed factors. This is rarely assumed, as most of the clinical studies are aimed at the population-level inference. In this case, the parameters to be inferred are only the within subject variances, as the between subject variance does not carry any statistical meaning.

Parametric approach - Mixed model + OLS & GLS

In the mixed model, the difference between the Ordinary Least Squares (OLS) and the General Least Squares (GLS) is how the within subject variance of the effect size is incorporated with the between subject variance of the effect size. In the former

method, the within subject variance are treated to be homogeneous, σ_w^2. The total variance for individual effect size would be $\hat{\sigma}_w^2 + \hat{\sigma}_{between}^2 = \hat{\sigma}_{OLS}^2$ for all subjects. In the GLS approach, the within subject variance are thought to be heterogeneous, and defined based on the variance of COPEs from the subject level. The total variance for the individual effect size would be $\hat{\sigma}_i^2 + \hat{\sigma}_{between}$ for the ith subject.

Only a single variance term, $\hat{\sigma}_{OLS}^2$, needs to be estimated in the OLS approach, making it a relatively simple estimation procedure. Another advantage is that the variance of the COPEs from the subject level is unneccesary, as the within subject variance are treated as homogeneous. The SPM software uses this approach and the OLS method in FSL uses this as well. For the GLS approach, the procedure is more complicated, since the total variance for each subject is heterogeneous - there are several options available for the estimation, such as restricted maximum likelihood or MCMC. For this approach, both the COPEs and the variance of COPEs from the subject level are required. In FSL, this is implemented as FLAME 1 and FLAME 2.

Obviously, the GLS approach is more accurate than the OLS approach, since it is reasonable to assume that the within subject variance is going to be different. Nevertheless, it is shown, at least in the one paired t-test context, that both approaches do not show significant difference [21]. Another point to consider is how the temporal autocorrelation of the errors at the subject level is propagated to the group level. As discussed in section 2.2.2, the COPEs, $c\hat{\beta}$ is going to be the same regardless of the degree of temporal autocorrelation as long as c, X, and Y are kept the same. The only affected quantity would be the variance of the COPEs. The intermediate conclusion is that the OLS is not affected by the autocorrelation, as only the COPEs are required for the estimation, whereas the GLS might be affected, as it requires the variance term for the estimation. Despite these pros and cons, the common standard in the fMRI field is to use the GLS approach over the OLS approach to account for the subject heterogeneity.

Nonparametric approach

In nonparametric approach at the group level, it is important to notice that the COPEs cannot be shuffled across the subjects, as these quantities are expected to be significantly different even under the null condition due to subject variability. The only permissible shuffling is the sign of the COPEs. Under the null distribution, the group average effect (in one sample t-test) or the difference between the group average effects (in two sample t-test or paired t-test) is expected to be zero, and the sign change should have no effect. For one sample t-test and a paired t-test, this means that there are only 2^N number of possible permutations, where N is the number of subjects. Since the null reference distribution is built from the permutations of COPEs, the variance of COPEs is not necessary for the nonparametric approach.

2.4.3 Group-level Inference with Multiple Comparisons

The multiple comparisons argument in section 2.3, which is focused on single subject case, can easily be extended to the multiple subject case. For the parametric approach, the procedure that first applies z-stat threshold and later the voxel threshold (calculated from Sidak correction) or the cluster threshold (calculated from GRF theory) is used in the same manner. The only difference is that the COPES and the variance of the COPEs are the group level parameters, $c\hat{\beta}_G$ and $var(c\hat{\beta}_G)$. For the nonparametric approach, the max statistic distribution is constructed from taking the max value of $\hat{\beta}_G$ from each iteration, which is estimated after shuffling the COPEs.

Chapter 3

Denoising

3.1 Brainstem Quality Control

The BOLD signals in the brainstem are more susceptible to physiological noise as the brainstem is located closer to the heart and therefore affected by more intense fluctuations, compared to the rest of the cortex [22]. Moreover, the nuclei in the brainstem, which are associated with numerous different neural circuits, are very small in size - if a ROI mask is misplaced by several voxels, the result will be completely different from what is expected. Therefore, extra caution is required for the brainstem BOLD signals. In this section, several aspects of the brainstem quality control are discussed.

3.1.1 Brainstem-specific Nuisance Regressors

Generally, the nuisance regressors are extracted from the cortical area, such as white matter cortex and CSF. As such, it is unclear as to how effective these regressors are in accounting for the noise affecting the brainstem. It is thus sensible to add nuisance regressors extracted from the regions in close proximity to the brainstem. Here, we consider two regions for extracting the brainstem-local nuisance regressors, the cerebellum white matter and the 4th ventricle.

Cerebellum WM Regressor

Cerebellum white matter, due to the fact that it is close to the brainstem and also that white matter only contains non-neuronal signals, was initially an appealing choice as a brainstem nuisance regressor. However, some properties of the cerebellum white matter make this an unfavorable candidate. Within the cerebellum, there are four nuclei called deep nuclei, which are clusters of gray matter lying within the white matter at the core of the cerebellum. The four nuclei - dentate, globose, emboliform, and fastigial - are the sole sources of output from cerebellum and each communicate with different parts of the brain and the cerebellar cortex. Therefore, when extracting the nuisance regressors from the cerebellum white matter, there is a risk of also including the neuronal BOLD signal as well. Moreover, the complicated structure of the cerebellum makes it hard to analyze what kind of neural processes, if at all, are reflected in the cerebellar BOLD signal [23].

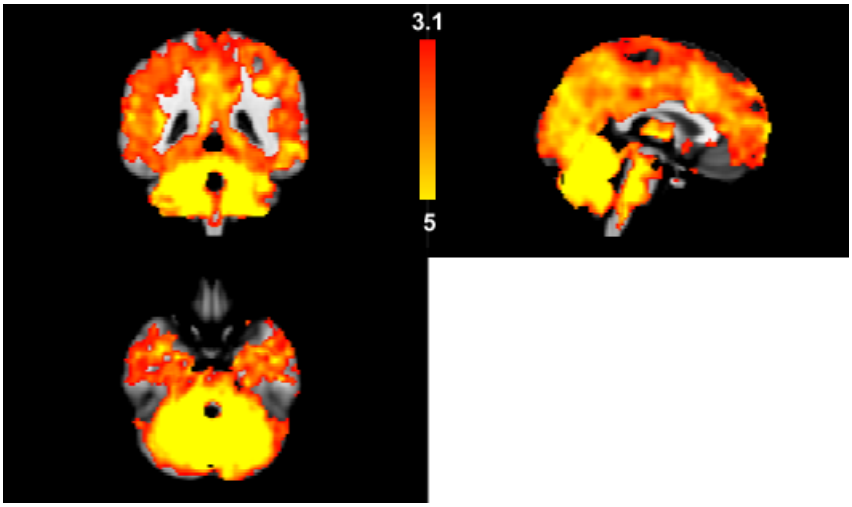

Figure 3-1: The group functional connectivity with the cerebellum white matter seed in pre state in MNI space (x=45, y=42, z=22).

Figure 3-1 and Figure 3-2 further corroborate the argument. The group functional connectivity with the cerebellum white matter seed in the pre state shows that the region is functionally connected with almost all parts of the cortical gray matter and the brainstem. This shows that the cerebellum white matter BOLD signal does contain neuronal signal as discussed previously. Therefore, the cerebellum white

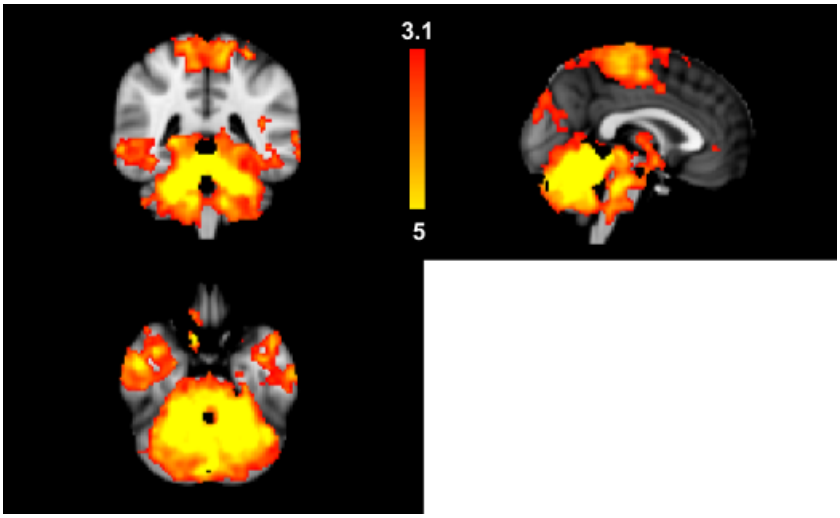

Figure 3-2: The group functional connectivity with the cerebellum white matter seed in peri state in MNI space (x=45, y=42, z=22).

matter signal would confound the result, rather than denoise the brainstem-specific noise as intended.

4th Ventricle Regressor

Figure 3-3 shows the seed used to extract the 4th ventricle ROI (33 voxels). It is important to note that the 4th ventricle is located dorsally to the Locus Coeruelus seed (in Figure 4-1) and thus requires extra caution not to include parts of the LC seed within the noise ROI mask. To ensure this, the extracted 4th ventricle signals are spatially unsmoothed.

Figure 3-4 and Figure 3-5 show the group functional connectivity with the 4th ventricle seed in pre and peri state, respectively. Both the pre and peri images show that the 4th ventricle region is mostly functionally connected with the adjacent parts of the cerebellum and the brainstem. Since the region is expected to only contain noise, the connected regions show the extent to which the noise affects the brainstem. The fact that there is no significant functional connectivity with the cortical noise ROIs supports the argument that the 4th ventricle noise is different (or uncorrelated) from the noise extracted from the cortical noise ROIs. In summary, these observations justify the inclusion of the nuisance regressors from the 4th ventricle region, as the

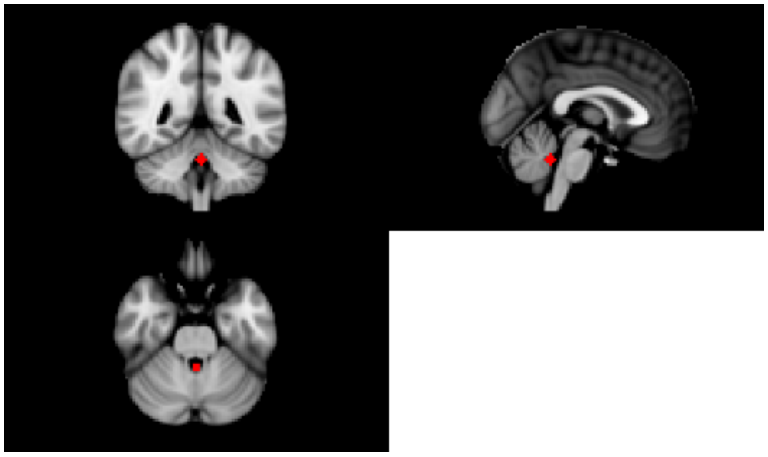

Figure 3-3: 4th ventricle seed (red) in MNI space (x=45, y=40, z=22)

means to denoise the brainstem-specific noise.

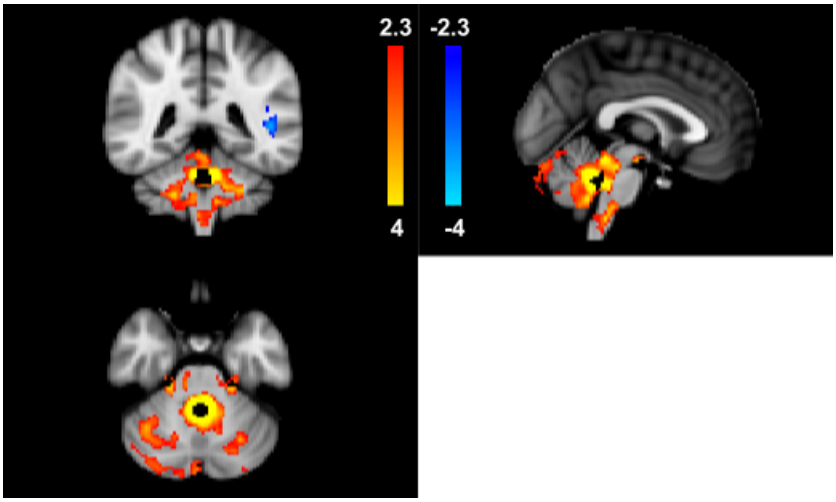

Figure 3-4: The group functional connectivity with the 4th ventricle seed in pre state in MNI space (x=45, y=42, z=21)

3.1.2 Laterality

The brainstem nucleus of our interest, the Locus Coeruleus, are consisted of two parts, right and left. Although it seems natural to assume that the BOLD signals in either side should be similar due to the symmetry, there are some factors to consider before drawing the conclusion. First, the structural variability between the individuals might result in asymmetric registration of the brainstem to the MNI space. Since the

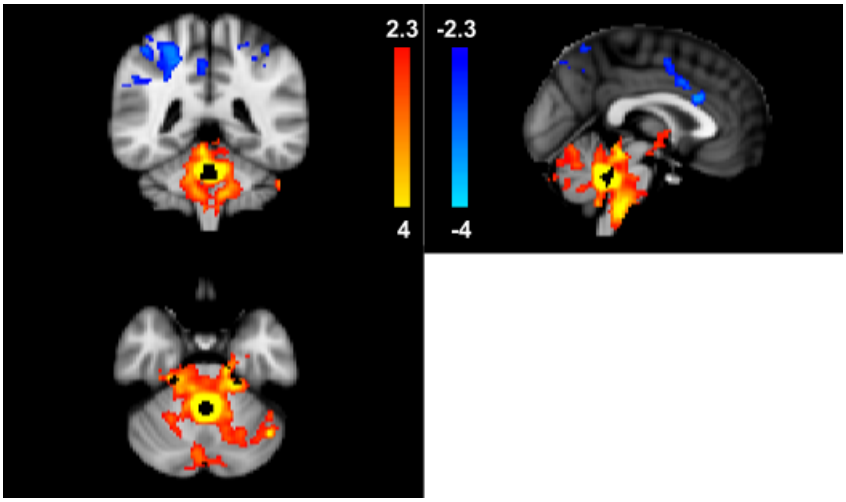

Figure 3-5: The group functional connectivity with the 4th ventricle seed in pre state in MNI space (x=45, y=42, z=21)

brainstem masks are defined in the MNI space, not in the individual structural space, these standard masks could include different regions for some individuals. Second, the movement artifacts or the pulsations in the ventricle region could have different effects on the either side. Finally, it is entirely possible that the left and the right nuclei exhibit different functional connectivity to the brain.

For these reasons, a quality control step to check the cross-correlation of BOLD signals between the voxels in the left and the right brainstem nuclei masks would be helpful. Ideally, the cross-correlation matrix would entirely be 1, which would mean that the BOLD signals are perfectly correlated not only within each mask, but also across the masks, indicating symmetry. For this dataset, this procedure was performed both on the LC mask. The LC mask on the MNI space had 20 voxels on both sides (40×40 cross-correlation matrix). The cross-correlation matrices were averaged over all subjects. Moreover, to check the effects of the denoising pipelines on the lateral regions, cross-correlation maps for three different preprocessing pipelines were created: (1) **Raw**: Raw signal without denosing (Figure 3-6) (2) **Avg**: Denoised signal with averaged nusiance regressors from WM, CSF, and 4th Ventricle regions (Figure 3-7) (3) **Compor**: Denoised signal with five principal components from WM,

CSF, and 4th Ventricle (Figure 3-8).

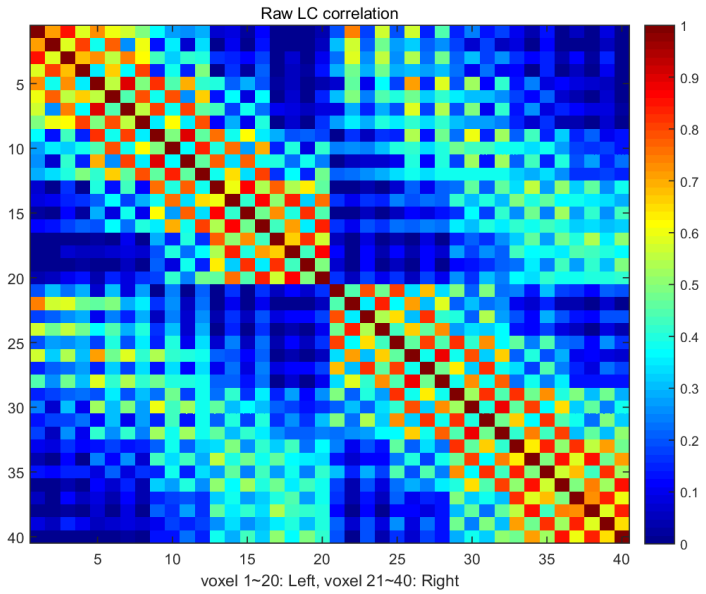

Figure 3-6: Cross-correlation matrix (averaged over subjects) for LC mask voxels without noise removal

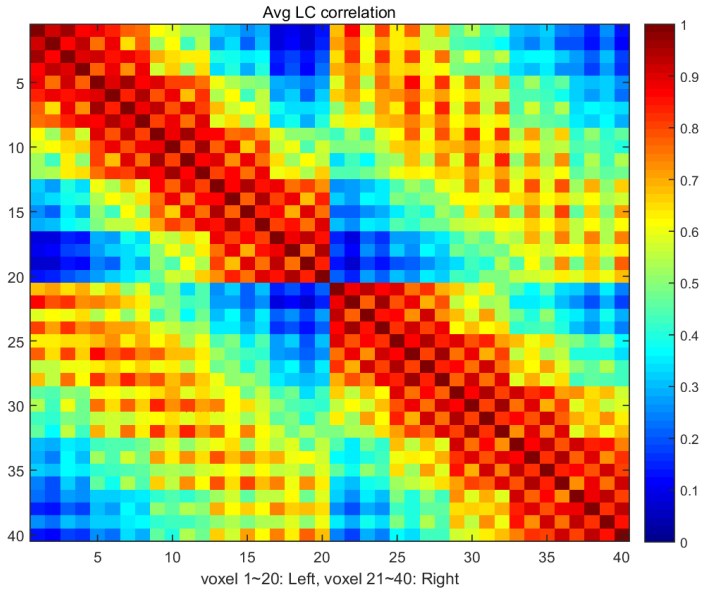

Figure 3-7: Cross-correlation matrix (averaged over subjects) for LC mask voxels denoised with averaged nuisance regressors from WM, CSF, and 4th Ventricle regions

It is easy to see that in LC seeds, the voxels can be quite uncorrelated without

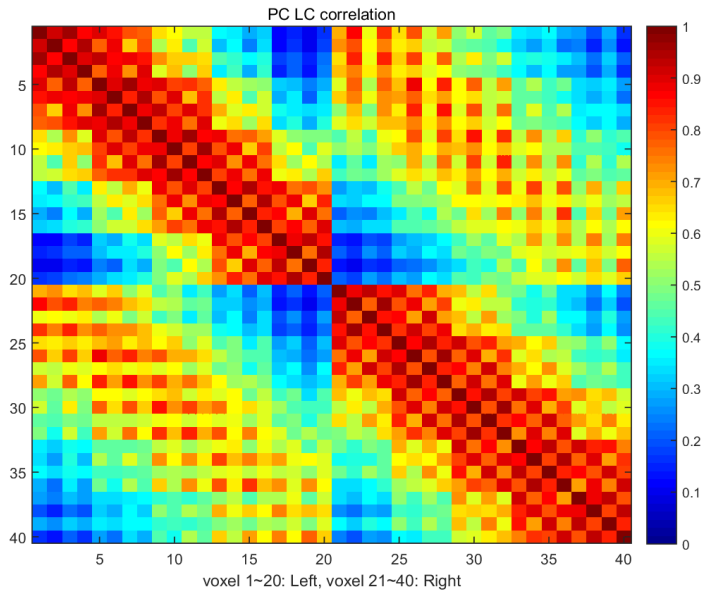

Figure 3-8: Cross-correlation matrix (averaged over subjects) for LC mask voxels denoised with principal nuisance regressors from WM, CSF, and 4th Ventricle regions

denoising, even within the same left or right masks, as in Figure 3-6. With some degree of denoising, we see marked increase in nearly all cross-correlation values, although we still see that the cross-correlation is not as strong across different lateral masks.

3.1.3 Spatial Smoothing

Since the brain nuclei are small, the conventional $5 \sim 6$mm FWHM spatial smoothing can result in including BOLD signals from adjacent nuclei, confounding the specificity of the functional connectivity. Some studies chose not to smooth the brainstem BOLD signal at all for this reason, while smoothing the cortex with the conventional kernel [24]. This ensures that there is some degree of smoothing in place, since the BOLD signals are averaged over the ROI mask. A systematic comparison between the different amounts of spatial somoothing shows that the FWHM of 1 or 1.5 voxels is appropriate [8].

For the Dexmedetomidine study, we chose minimum spatial smoothing with the

FWHM of 1.5 voxel, or 3mm. This was preferred over the unsmoothing scheme, as we expected some amount of spatial smoothing to account for the BOLD signals of the adjacent voxels that could have been left out of the ROI masks.

3.2 Principal Component Approach

3.2.1 Is Principal Components for noise removal effective?

As previously discussed, there are several methods of denoising, without any clear explanations of which one is better than the other. Due to its simplicity, using averaged regressors from the noise ROIs has been popular; ICA-based approach has also been gaining popularity as it is readily implemented for use. Here, we focus on denoising via the principal component based approach.

There are two important assumptions that enable the noise ROI-based nuisance regression approach. First is that the ventricle and the white matter regions contain BOLD signal only of non-neuronal origin. The second assumption is that the noise structure observed in the noise ROI is prevalent throughout the entire brain. If the underlying structure for the noise were to be radically different in some brain regions from that of the noise ROI, this approach would be less effective. This of course, is not to conclude that denoising with signals or components derived from the noise ROIs produces complete noise-free BOLD signal in Gray Matter region. Nevertheless, this is the best we can do without external physiological measurements or additional information.

Under these assumptions, the most rudimentary method would be to include the BOLD signal from every voxel in the noise ROI as the nuisance regressors. Such model would account for the common underlying noise structure as well as small noise sources that cause subtle differences between the BOLD signals. As one could suspect, this is never feasible due to the issues of degree of freedom. Normally, the number of scans is on the scale of hundreds, whereas the number of voxels in the noise ROIs are well over the scale of thousands, resulting in negative DOF. Even if the number of scans was greater than the number of voxels, the computation would be very expensive.

Thus, the idea is to reduce the number of regressors within the range of suitable DOF and also ensure that these regressors capture the essence of the noise. The simplest approach is averaging every voxel in each noise ROI to get a single nuisance regressor. This approach is based on the idea that pooling over different BOLD signals would yield a representative noise signal. The idea of averaging, due to its simplicity, is prevalent not only in the neuroimaging research, but also in most of the fields involving timeseries analysis. Nevertheless, there remains a doubt as to whether the procedure causes information loss, as subtle details existent only in some subset of voxels could be averaged out and thus not accounted for. This is the motivation for the principal component based approach, as we are able to include additional representative signals as nuisance regressors. The remaining section looks at how the principal component based approach compares with the averaged regressor approach and also the additional insights provided by the method.

Comparison between the averaged regressor and the principal component approach

To assess how different the averaged regressor and the principal component regressors are, we ran a cross-correlation between these regressors for each subject. The expectation was that the first few principal components would be correlated with the averaged regressors, as these were expected to capture the dominant nuisance signals respectively.

Figure 3-9 and Figure 3-10, which are the averaged cross-correation matrices for pre and peri condition respectively, confirm the initial prediction in a stronger fashion. The first principal component regressor for each noise ROI (WM: #2, CSF: #8, 4th Ventricle: #14) is almost perfectly correlated with the averaged regressors from respective regions (WM: #1, CSF: #7, 4th Ventricle: #13), with the exception of the CSF region, which still shows high correlation of around 0.7. Since the almost perfect correlation between two regressors means that these regressors are very sim-

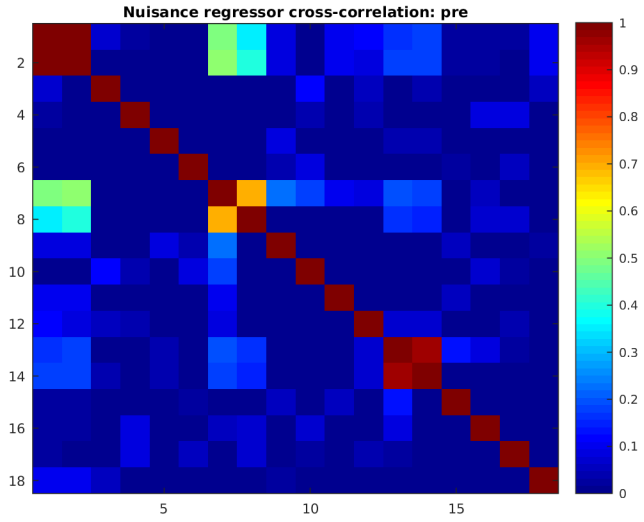

Figure 3-9: Cross-correlation matrix (averaged over subjects) in pre condition between nuisance regressors - #1: WM averaged, #2∼#6: WM principal components, #7: CSF averaged, #8∼#12: CSF principal components, #13: 4th ventricle averaged, #14∼#18: 4th ventricle principal components

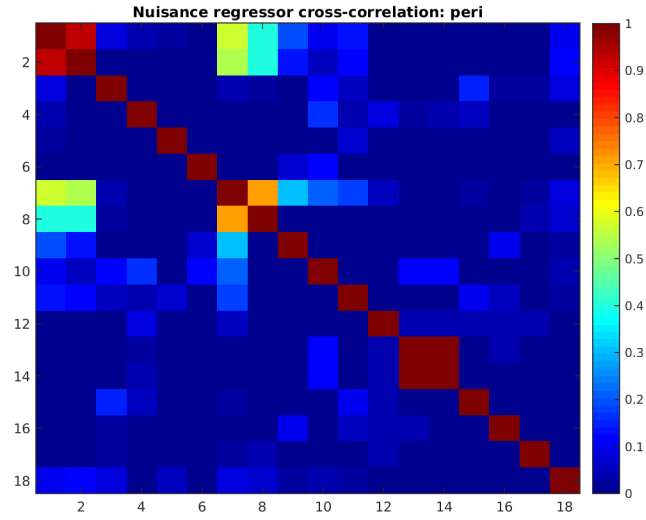

Figure 3-10: Cross-correlation matrix (averaged over subjects) in peri condition between nuisance regressors - #1: WM averaged, #2∼#6: WM principal components, #7: CSF averaged, #8∼#12: CSF principal components, #13: 4th ventricle averaged, #14∼#18: 4th ventricle principal components

ilar, we can state that the first principal component of each noise ROIs extract the same signal as that captured by the averaged regressor, almost exactly. Figure 3-11

shows an example of this statement. The averaged regressor and the first principal component, both extracted from WM, are almost the same, whereas the second principal component is uncorrelated with the first, as expected. This observation allows us to further conclude that several principal components as a whole is guaranted to include more noise signal than the averaged regressor, since the first principal component is almost equivalent to the averaged regressor, and thus the additional principal component regressors would add more noise information not already accounted for. As an additional comment, the cross-correlation between the principal component regressors within each noise ROI should be zero, as expected from the properties of the Principal Component Analysis.

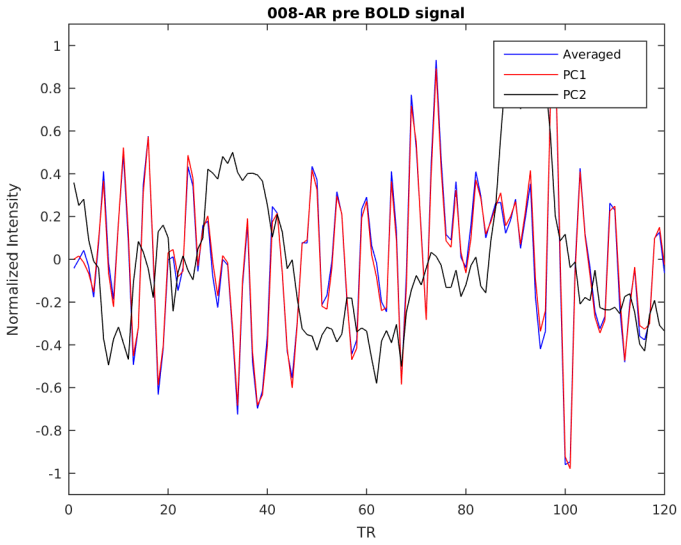

Figure 3-11: Averaged, the first principal component, and the second principal component regressors of 008-AR White Matter in pre condition. The averaged regressor and first principal component regressor are almost the same. All timeseries are normalized so that the maximum intensity is 1.

Subject Variability in variance explained by Principal Components

Due to subject variability, the kth principal component of noise ROIs will explain different amounts of variance for each subject. This is demonstrated by Figure 3-

12 ∼ Figure 3-19, where the accumulated explained variance is plotted against the number of principal components for different conditions and noise ROIs. Here, the 15 subjects are divided into two groups for increased visibility.

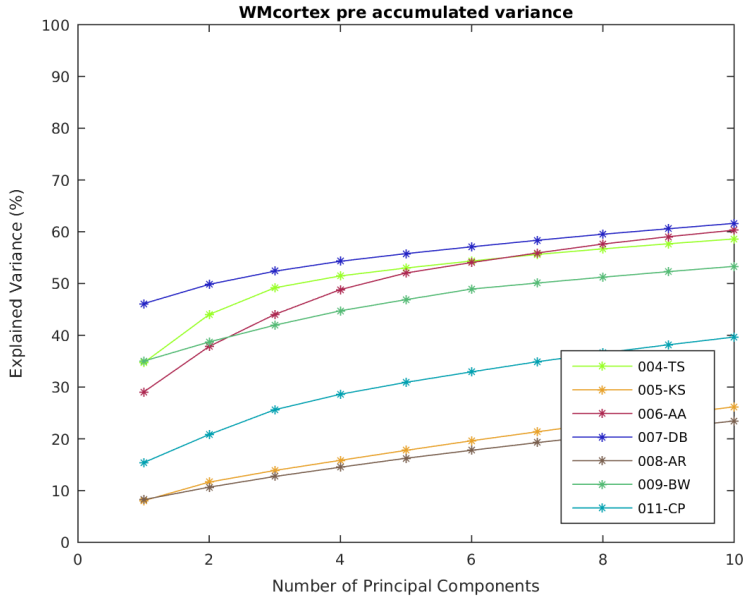

Figure 3-12: WM cortex accumulated explained variance plotted against the number of principal components in pre condition for 7 subjects

It is easy to observe that the subject variability in terms of the accumulated explained variance is quite big. In Figure 3-12, the first two principal components are able to explain about 50% of the variance for subject 007-DB, whereas the first ten principal components are barely able to explain about 30% of the variance for subject 005-KS. However, these observations are not consistent across different conditions, as in Figure 3-13, or the peri condition, - principal components in 005-KS are able to explain more variance than 007-DB.

It is not apparent why such individual variability exists, or more specifically, what is implied by the different magnitudes of explained variances. One possible explanation is that the explained variance somehow indicates how 'structured' the brain states are in general. If the first few principal components, or the first principal component specifically, explain great amount of total variance, this means that much of the brain

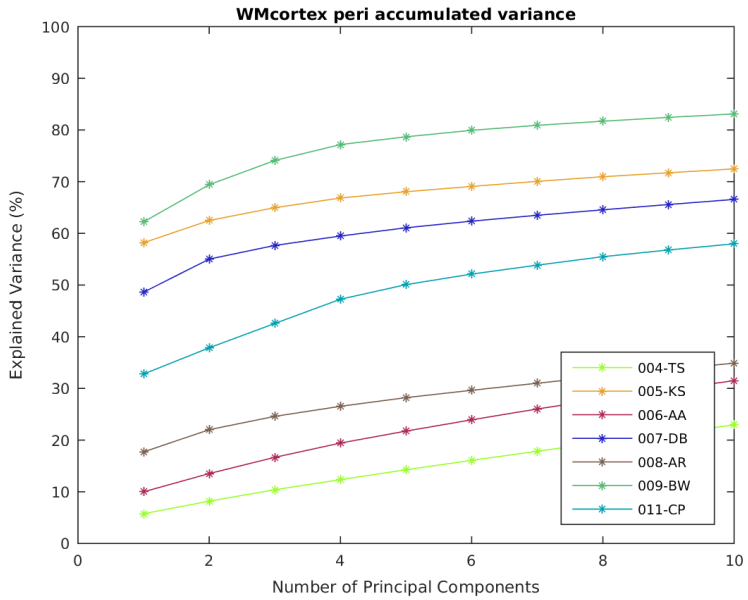

Figure 3-13: WM cortex accumulated explained variance plotted against the number of principal components in peri condition for 7 subjects

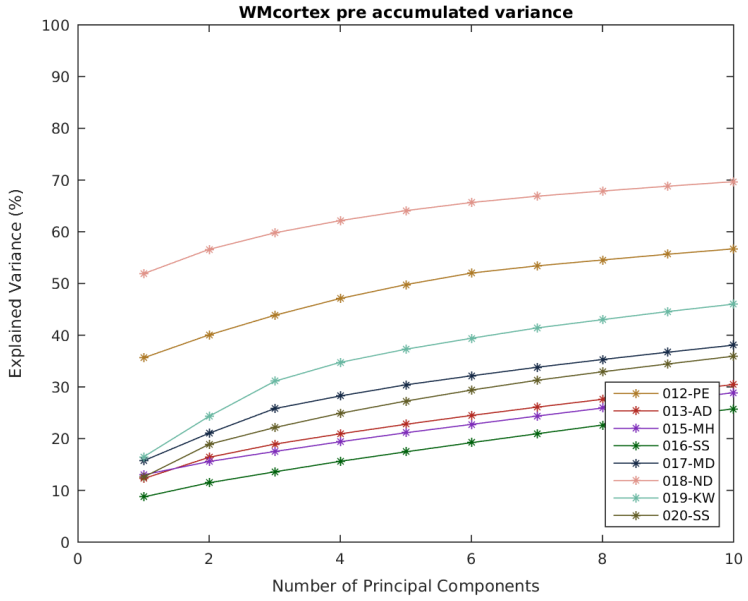

Figure 3-14: WM cortex accumulated explained variance plotted against the number of principal components in pre condition for 8 subjects

BOLD signals can be explained by some linear combination of the principal components. Stated differently, these principal components could be treated as underlying signals that explain much of the variance in the noise ROI.

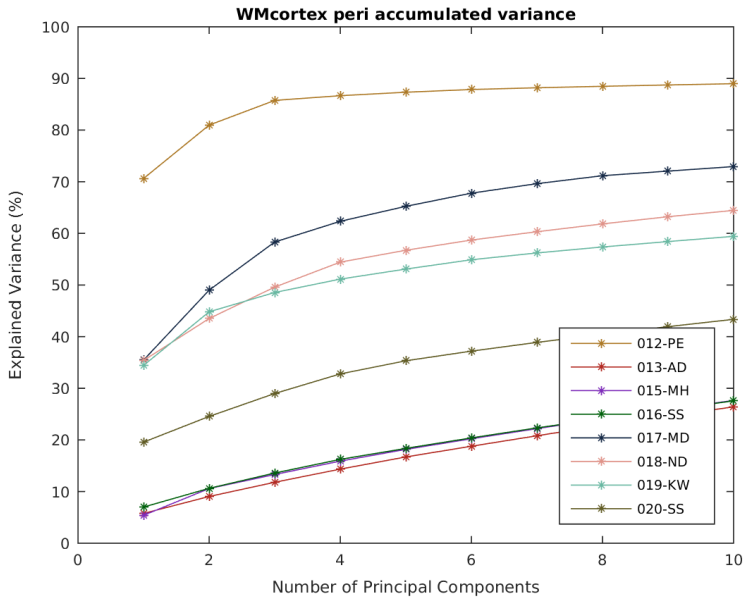

Figure 3-15: WM cortex accumulated explained variance plotted against the number of principal components in peri condition for 8 subjects

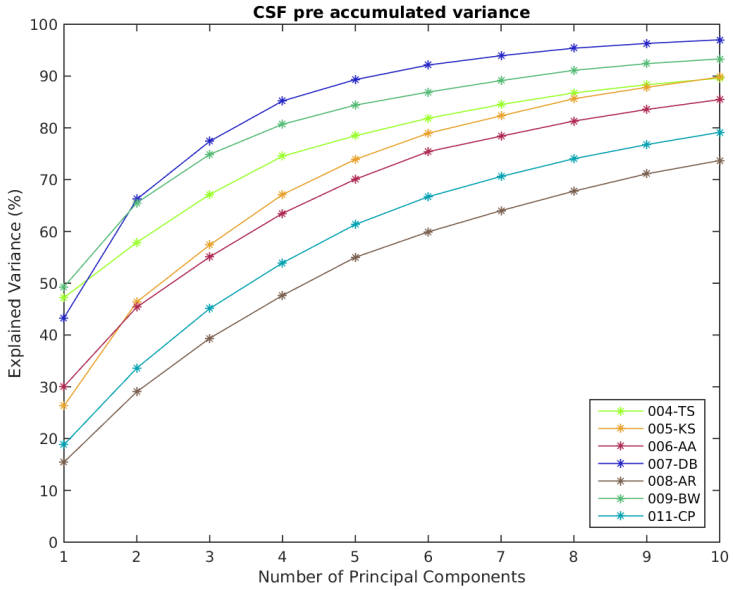

Figure 3-16: CSF accumulated explained variance plotted against the number of principal components in pre condition for 7 subjects

However, if the explained variance by the first few principal components is low, such as 004-TS in Figure 3-13, the brain structure would be less structured. If PCA was

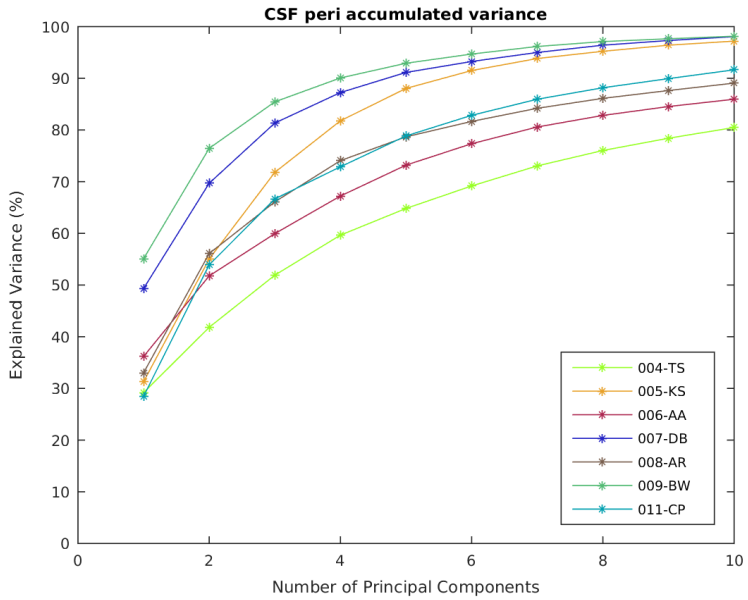

Figure 3-17: CSF accumulated explained variance plotted against the number of principal components in peri condition for 7 subjects

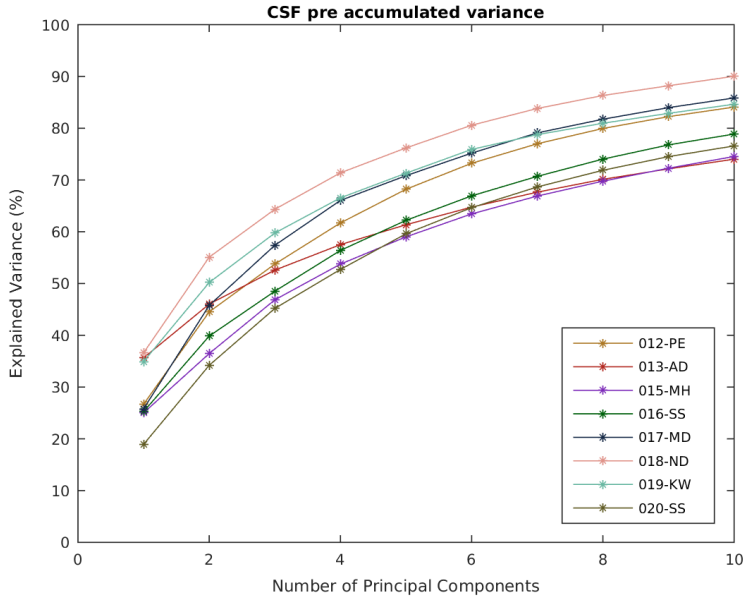

Figure 3-18: CSF accumulated explained variance plotted against the number of principal components in pre condition for 8 subjects

to be run on the dataset and the different principal component is chosen as the first principal component and all others components subsequently, the trend between the accumulated explained variance and the number of principal components would be

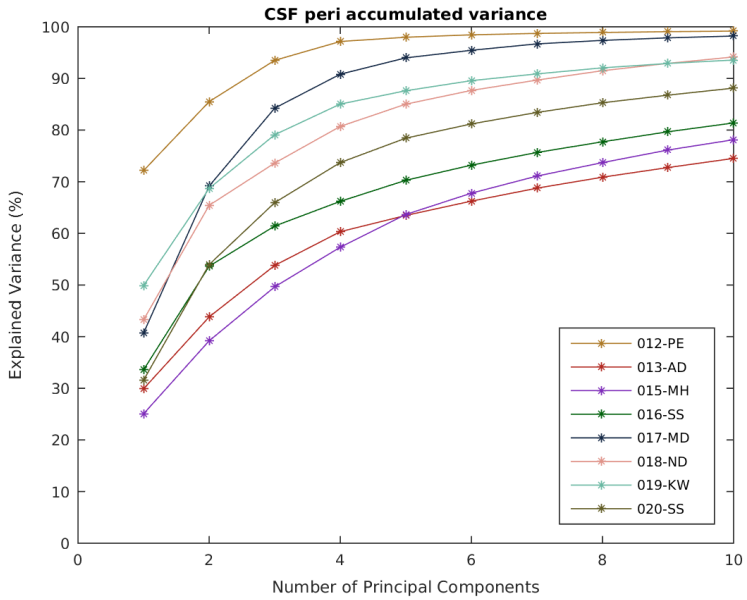

Figure 3-19: CSF accumulated explained variance plotted against the number of principal components in peri condition for 8 subjects

similar. Since there is no dominant principal component in this sense, any principal component could be treated as the underlying signal, implying that the brain BOLD signals are relatively unstructured. This is actually the idea behind the Bartlett's test for sphericity [25]. A structured dataset, with few dominating eigenvalues, would form hyperellipsoid, oblong along the dominant principal components, whereas an unstructured dataset would form a shape close to a sphere.

This brings up a crucial question: What factors give rise to the structured and unstructured signal? How do these factors affect the subjects differently in the pre, peri, and post states? At this point, without more sophisticated measurements, we can only make speculations about the underlying factors. Here are some possible explanations:

1) Since cardiac/respiratory noise is periodic, it can be treated as a structured signal. 2) Movement artifacts can both be structured and unstructured. It is structured in a sense that the whole brain is shifted by similar amount, but unstructured in a sense that movements can cause nonlinear effects throughout the brain.

3) Since the brain state is expected to be more stable and structured under anesthesia (or unconscious states), it is expected that more variance is explained by the same set of principal components in the peri state than the pre state. The comparison between the pre and peri plots seems to support the argument, albeit not clearly. Although the average explained variance is increased, some subjects have decreased explained variance, such as 004-TS and 006-AA in Figure 3-12 and Figure 3-13.

Noise ROI Variability in variance explained by Principal Components

Another observation is that the type of noise ROIs also causes the amount of explained variance to be different for same subject. Fewer number of principal components are required to explain certain amount of the total variance in CSF than WM cortex. This was also noted in the other work on the principal component approach, where the mean number of principal components to explain 50% variance of the signal was 17.9 (standard deviation: 9.8) for WM and 3.0 (standard deviation: 1.1) for CSF [26]. Although not included in this work, even fewer numbers are required for the 4th ventricle ROI. In lieu of the previous structured signal argument, we could conclude that the CSF region is more 'structured' than the WM region. However, there are no plausible biophysical explanations yet.

3.2.2 Effective number of Principal Components

Typically, about five principal components from each noise ROI are included as nuisance regressors [15]. This decision is bsed on the broken stick method [25], which examines the eigenvalues of the principal components to see whether some significant signal is captured by the eigenvectors as opposed to normally distributed random noise. According to this method, the mean of five principal components was sufficient to include non-trivial signal, or axis in the context of PCA, from noise ROI. There has also been a study that systematically examines the effect of different number of principal components, from a single to ten components [12]. This study concluded that, although including higher number of principal components seems to result in

more effective noise correction, there is a diminishing return, reflected in the reduction of the correlational strengths, suggesting that the five principal components is recommended. Another study focused on how many principal components would be required individually to explain 50% of total noise variance from the noise ROI and compared this approach with the five principal component approach [26]. Apart from some subtlety, the results were not significantly different, further attesting to the sufficiency of five principal components.

Nevertheless, this does not entirely settle the argument on the effective number of principal components. as some crucial questions are left unanswered. If the first five principal components are able to explain some percentage of the total signal variation in the noise ROI, what does the remaining unexplained variation mean? Since the signal is extracted from the noise ROI, the unexplained variance should also have the noise characteristics. Including as many principal components as possible to explain more variation, for example 50% of total variation, is impractical since the reduction in the degree of freedom is too significant. Recall that the total degree of freedoms in GLM is constrained by the number of TRs, which is normally set to be around 100 scans. Now, what if the unexplained variance includes crucial structured noise other than random Gaussian noise, not accounted otherwise? In addition, as the amount of variance explained by a specific number of principal components is different from subject to subject, what is the implication for the group-level inference, when the individual results are pooled together to draw a group-level conclusion? This brings us back to the fundamental question of finding a sufficient denoising strategy.

3.2.3 Several interpretations of Principal Components

As the previous results show, the first principal component from the noise ROI matches the averaged regressor of the noise ROI, and it is thus possible to give a meaningful interpretation to the first principal component. Nevertheless, interpreting the rest of the principal components from the noise ROI is not so intuitive, other than that these explain the most variance in a sequential manner. It is possible that

some principal components capture the nonlinear interactions between the physiological processes, or even a single physiological process alone. The point is that, as in other applications of PCA, it is hard, and maybe meaningless, to make sense of what each principal component represents, since the technique is purely based on the data without external information.

One possible interpretation of the principal components based approach is by examining the power spectra of raw and denoised BOLD signals in the noise ROIs. Figure 3-20 $\sim$ Figure 3-23 show how different number of principal components affect the denoised power spectra. The spectra are averaged over all the voxels in the WM and CSF and only temporal filter (HPF with cut-off frequency of 0.008 hz) is applied to the raw signal. Numbers represent the number of principal components included as the nuisance regressors.. As the number increases, the resulting spectra roughly becomes flatter, or closer to the white noise. Note that the averaged regressor result closely resembles the first principal component regressor result. Also, the raw signal spectra roughly follows the $1/f$ pattern, as noted in many literatures.

If the spectra, or the power spectral density (PSD), of the signal is flat, there is no autocorrelation (or minimum autocorrelation, since the spectra is not perfectly flat). From this perspective, the denoising pipeline removes the noise components that are autocorrelated in the noise ROIs, leaving roughly uncorrelated noise signal as the result. The more the principal components, the more the autocorrelation seems to be removed, since the spectra becomes flatter. However, beyond some number of components, the shape of the spectra is roughly kept the same, with only the intensity becoming smaller, suggesting that beyond some point, including more principal components is similar to subtracting white noise from the signal.

Since the functional connectivity between the intrinsic brain networks involves intrinsic autocorrelation in the BOLD signal, if the denoising can remove non-neuronal autocorrelation from the signal, or in other words, autocorrelation in the noise ROIs, we could be confident that the resulting signal is almost noise-free. The principal

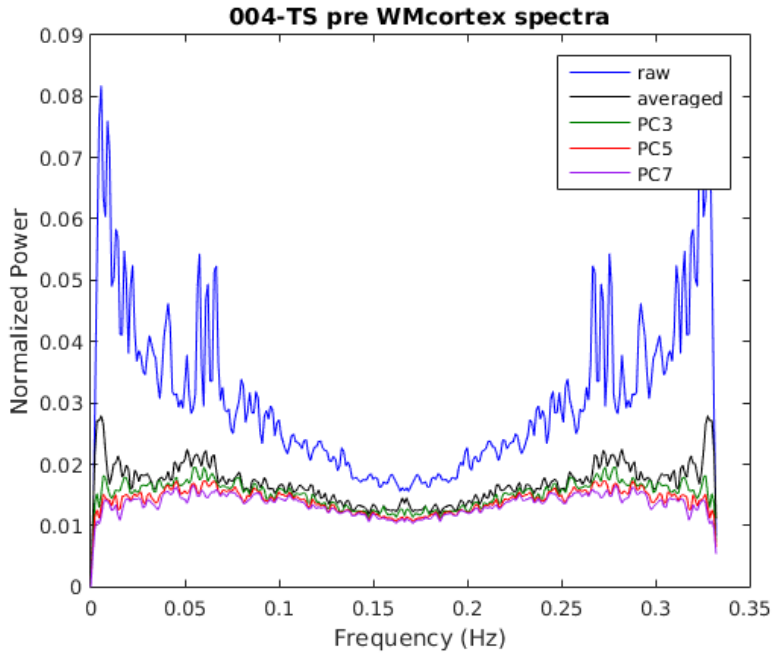

Figure 3-20: White Matter cortex spectra for a subject (004-TS) with different denoising schemes.

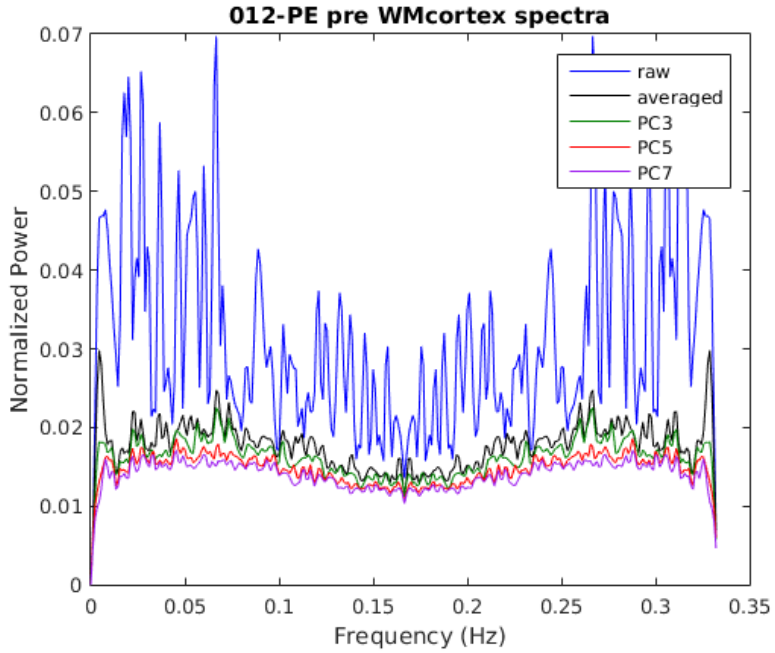

Figure 3-21: White Matter cortex spectra for a subject (012-PE) with different denoising schemes.

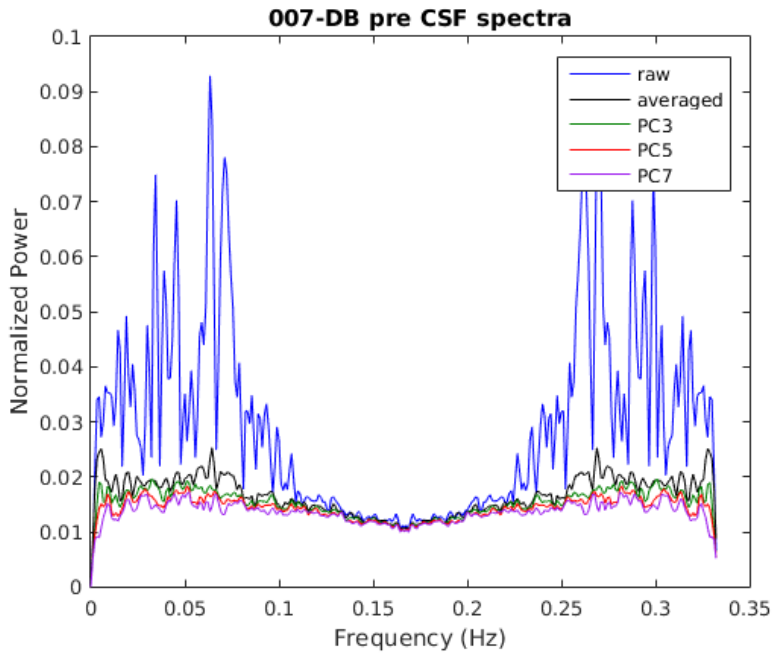

Figure 3-22: White Matter cortex spectra for a subject (007-DB) with different denoising schemes.

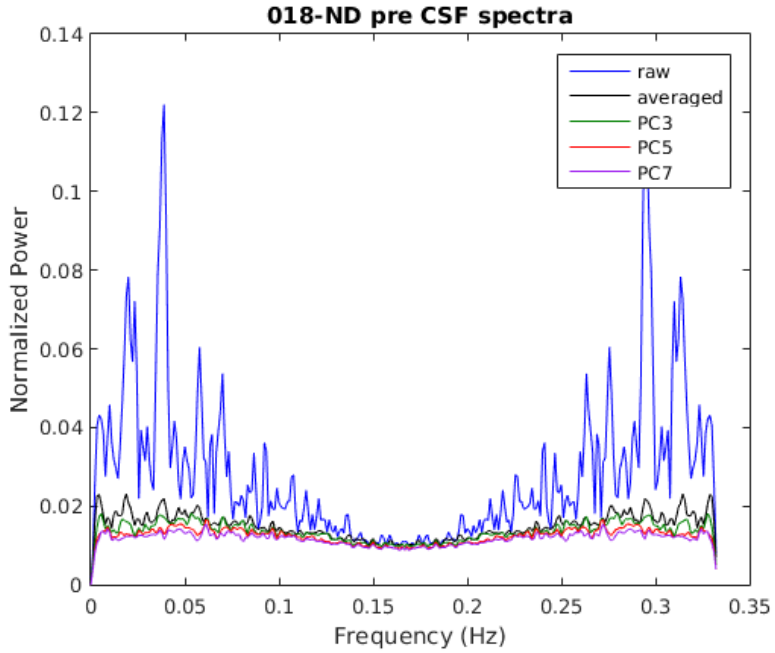

Figure 3-23: White Matter cortex spectra for a subject (018-ND) with different denoising schemes.

component based approach can perform the task on the same level or better than the averaged regressor approach. Nevertheless, one should try to find the appropriate number of principal components, as there exists a tradeoff between the degree of freedom and the flatness of the resulting spectra in the noise ROI.

The drawbacks of this approach are, 1) since the Nyquist Frequency is low for this analysis (0.17Hz), aliasing could be the confouding factor in assessing the flatness of the spectra and 2) the analysis needs to be done more rigorously, to quanitfy the flatness of the spectra with some metric (for instance, Wiener entropy).

In conclusion, the previous discussions give us confidence in preferring the principal component approach over the averaged apporach, in the absence of the sureproof metric for the comparison of the two denoising schemes.

Chapter 4

Application to fMRI data

4.1 Functional connectivity between the brainstem and the brain under Dexmedetomidine

In this section, we discuss the results on functional connectivity between the brainstem nucleus, Locus Coereleus (LC), in altered arousal states by Dexmedetomidine, produced by different pipelines. As mentioned in 1, Dexmedetomidine is of great clinical interest and specifically targest LC nucleus. Figure 4-1 represents the mask used to extract ROI signals from LC. The mask was drawn based on the probabilistic atlas of LC [27].

All the necessary preprocessing steps were preformed on the Dexmedetomidine dataset, including brain extraction, slice-time correction, B0 correction, temporal filtering, and registration onto MNI space. 5 principal components with highest eigenvalues each from the eroded masks of cortical WM and CSF, and 1 principal component from the eroded 4th ventricle mask were included as nuisance regressors for each subject's GLM. The noise ROI nuisance regressors were extracted from the spatially unsmoothed data, to further minimize the possibility of the inclusion of the gray matter neuronal signal. The brainstem was spatially smoothed with 3mm FWHM and the rest of the brain was spatially smoothed with 5mm FWHM. The regressor of interest was extracted from the LC mask. Along with 6 motion regressors,

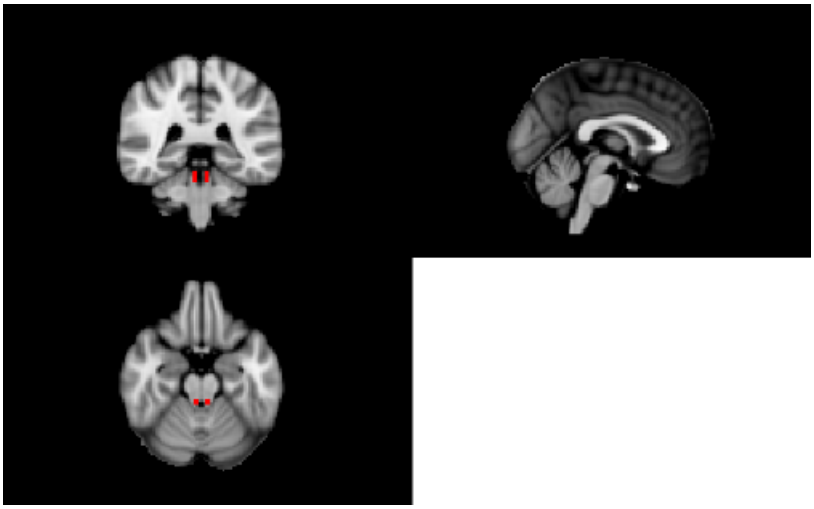

Figure 4-1: Coronal, Sagittal, and Transverse view of the Locus Coereleus seed (red) in MNI space (x=54, y=44, z=25)

the total number of regressors in the GLM ended up being 18, with one regressor of interest and 17 nuisance regressors. The COPEs and the variance of COPEs for the regressor of interest for each subject were passed onto the group level analysis.

For the individual condition group analysis (Figure 4-2, Figure 4-3, and Figure 4-4), one sample t-test was used with the initial z-stat threshold of 3.1 and the cluster size threshold for FWER of 0.05. For the contrast between two different conditions, peri and pre & post and peri (Figure 4-5 and Figure 4-6), paired t-test was used with the initial z-stat threshold of 2.3 and the cluster size threshold for FWER of 0.05.

It is interesting to see which regions have decreased functional connectivity with LC in the Dexmedetomidine-anesthetized state. The Posterior Cingulate Cortex (PCC), Medial Prefrontal Cortex (MPFC), Thalamus, and Putamen are such regions. Since the thalamo-cortical functional connectivity is also disrupted when the subject is unconscious due to Dexmedetomidine [2], it makes sense that the functional connectivity between LC and Thalamus, and LC and PCC are decreased. These regions seem to regain functional connectivity in the recovery state (post) as can be observed from Figure 4-6. Nevertheless, only small portion of Thalamus/Putamen and even smaller portion of PCC are recovered, which is expected by the fact that

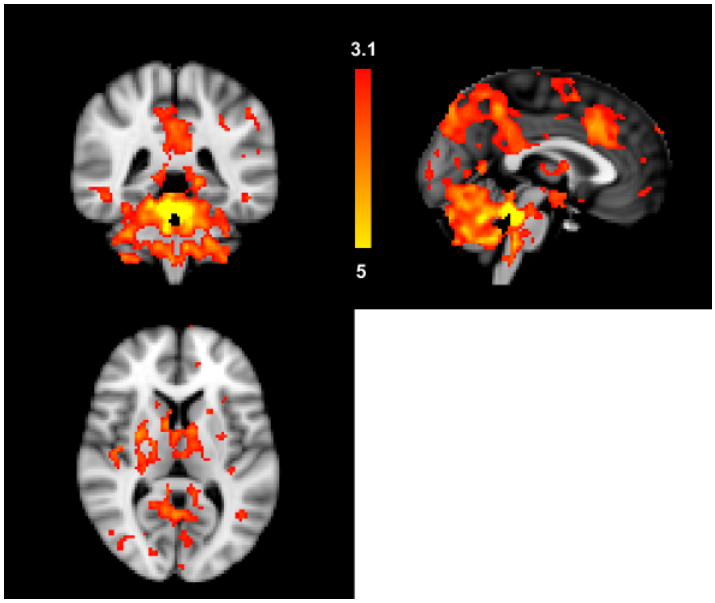

Figure 4-2: Coronal, Sagittal, and Transverse view of the LC functional connectivity in pre condition in MNI space (x=45, y=43, z=40)

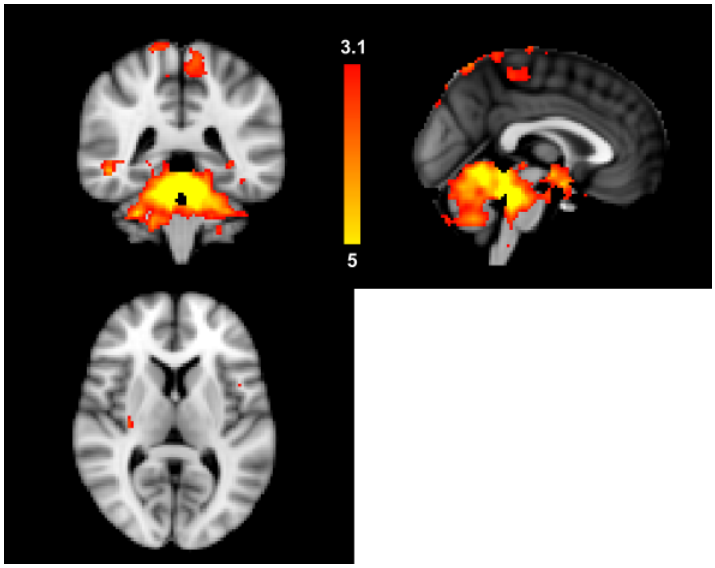

Figure 4-3: Coronal, Sagittal, and Transverse view of the LC functional connectivity in peri condition in MNI space (x=45, y=43, z=40)

the subjects are not fullly recovered. These findings are further supported by the neuroanatomical findings. As with many other brainstem nucleus, LC projects to the Thalamus. In addition, The LC projects to the anterior and posterior cingulate cortex [28]. Therefore, it would be a natural conclusion that Dexmedetomidine binding to α2-adrenergic receptors affects the afferent conenction to both the Thalamus and

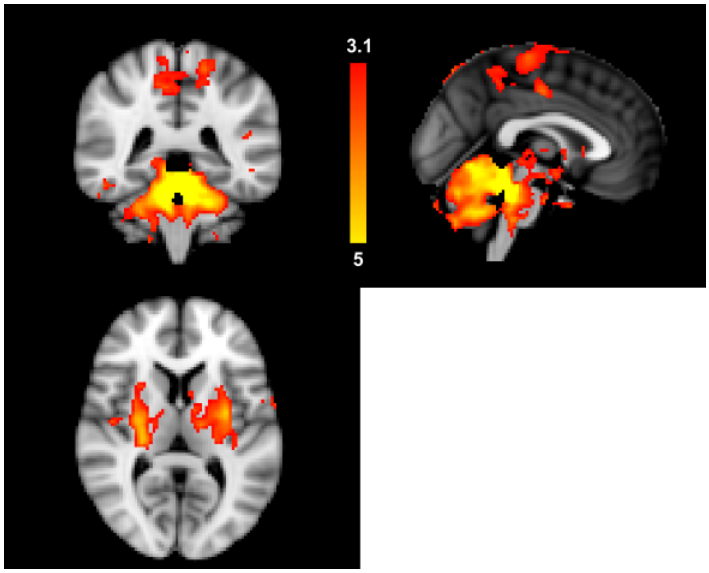

Figure 4-4: Coronal, Sagittal, and Transverse view of the LC functional connectivity in post condition in MNI space (x=45, y=43, z=40)

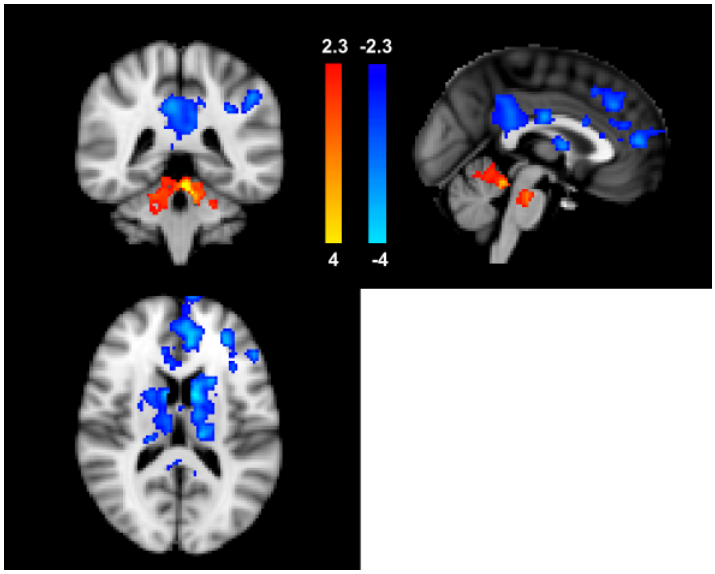

Figure 4-5: Coronal, Sagittal, and Transverse view of the LC functional connectivity in the contrast image of peri and pre in MNI space (x=45, y=43, z=43)

PCC and therefore result in decreased functional connectivity.

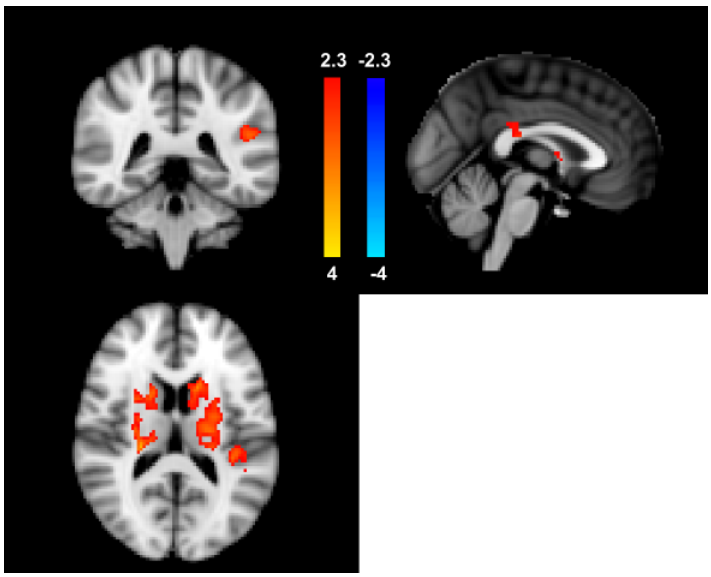

Figure 4-6: Coronal, Sagittal, and Transverse view of the LC functional connectivity in the contrast image of post and peri in MNI space (x=45, y=43, z=43)

Bibliography

[1] E.N. Brown et al., "General Anesthesia, Sleep, and Coma," *New England Journal of Medicine* vol. 363, pp. 2638-2650, 2010.

[2] O. Akeju et al.,"Disruption of thalamic functional connectivity is a neural correlate of dexmedetomidine-induced unconsciousness," *eLife*, 3:e09215, 2014.

[3] R.L. Buckner et al., "The brainâĂŹs default network: anatomy, function and relevance to disease," *Ann. N Y Acad. Sci.* vol. 1124, pp. 1âĂŞ38, 2008.

[4] C. Chang, G. H. Glover, "TimeâĂŞfrequency dynamics of resting-state brain connectivity measured with fMRI," *NeuroImage*, vol. 50, pp. 81âĂŞ98, 2010.

[5] G.L. Gerstein, D.H. Perkel, "Simultaneously Recorded Trains of Action Potentials: Analysis and Functional Interpretation," *Science*, vol. 164, pp. 828-830, 1969.

[6] K.J. Friston et al., "Functional connectivity: The principal component analysis of large (PET) data sets," *J. Cereb. Blood Flow Metab.*, vol. 13, pp. 5-14, 1993.

[7] Y. Yue et al., "Adaptive spatial smoothing of fMRI images," *Statistics and its interface*, vol. 3, pp. 3-13, 2010.

[8] F. Beissner et al., "fMRI of the brainstem using dual-echo EPI," *Neuroimage*, vol. 55, pp. 1593-1599, 2011.

[9] G. Kruger et al., "Neuroimaging at 1.5 T and 3.0 T: comparison of oxygenation-sensitive magnetic resonance imaging," *Magn. Reson. Med.*, vol. 45, pp. 595âĂŞ604, 2001.

[10] Purdon P, Weisskoff R "Effect of temporal autocorrelation due to physiological noise and stimulus paradigm on voxel-level false-positive rates in fMRI," *Human Brain Mapping*, vol. 6, pp. 239-249, 1998.

[11] T. Hastie et al., *The Elements of Statistical Learning*, 3rd ed., Springer, 2011.

[12] X.J. Chai et al., "Anticorrelations in resting state networks without global signal regression," *Neuroimage*, vol. 59, pp. 1420âĂŞ1428, 2012.

[13] C.C. Chen, C.W. Tyler. "Spectral Analysis of fMRI Signal and Noise," in *Novel Trends in Brain Science*, Springer, 2008.

[14] A. Hayen et al., "The effects of altered intrathoracic pressure on resting cerebral blood flow and its response to visual stimulation," *Neuroimage*, vol. 66, pp. 479-488, 2013.

[15] Y. Behzadi et al., "A component based noise correction method (CompCor) for BOLD and perfusion based fMRI," *Neuroimage*, vol. 37, pp. 90âĂŞ101, 2007.

[16] G.H. Glover et al., "Image-Based Methods for Retrospective Correction of Physiological Motion Effects in fMRI: RETROICOR," *Magnetic Resonance in Medicine*, vol. 44, pp. 162-167, 2000.

[17] Worsley, K.J. e al., "A unified statistical approach for determining significant signals in images of cerebral activation," *Human Brain Mapping*, vol. 4, pp. 58-73, 1996.

[18] A.M.Winkler et al., "Permutation inference for the general linear model," *Neuroimage*, vol. 92, pp. 381-397, 2014.

[19] F. G. Ashby, *Statistical Analysis of fMRI Data*, MIT Press, 2011.

[20] J.A. Mumford, et al., "Modeling and inference of multisubject fMRI data," *IEEE Engineering in Medicine and Biology Magazine*, vol. 25, pp. 42-51, 2006.

[21] J.A. Mumford, T.E. Nichols, "Simple group fMRI modeing and inference," *Neuroimage*, vol. 47, pp. 1469-1475, 2009.

[22] J.C.W. Brooks et al., "Physiological Noise in Brainstem fMRI," *Frontiers in Human Neuroscience*, 7:1âĂŞ13, 2013.

[23] J. Diedrichsen et al., "Advances in functional imaging of the human cerebellum," *Current Opinion in Neurology*, vol. 23, pp. 382-387, 2010.

[24] V.P. Murty et al., "Resting state networks distinguish human ventral tegmental area from substantia nigra," *NeuroImage*, vol. 100, pp. 580âĂŞ589, 2014.

[25] D.A. Jackson, "Stopping rules in Principal Component Analysis: A Comparison of Heuristical and Statistical Approaches," *Ecology*, vol. 74, pp. 2204-2214, 1993.

[26] J. Muschelli, "Reduction of motion-related artifacts in resting state fMRI using aCompCor," *Neuroimage*, vol. 96, pp. 22-35, 2014.

[27] T.P. Naidich et al., *Duvornoy's Atlas of the Human Brain Stem and Cerebellum*, Springer, 2009.

[28] Deepak N. et al., *Cerebral Cortex - Volume 4: Association and Auditory Cortices*, Springer, 1985.